FULL POLARIMETRIC NON-SPECULAR SCATTERING OF FLAT PLATE STRUCTURES THESIS

Jeffrey L. Fath, B.S.E.E.
Second Lieutenant, USAF

AFIT/GE/ENG/86D-26

DEPARTMENT OF THE AIR FORCE
AIR UNIVERSITY
AIR FORCE INSTITUTE OF TECHNOLOGY

Wright-Patterson Air Force Base, Ohio

AFIT/GE/ENG/86D-26

FULL POLARIMETRIC NON-SPECULAR SCATTERING OF FLAT PLATE STRUCTURES
THESIS

Jeffrey L. Fath, B.S.E.E.
Second Lieutenant, USAF

AFIT/GE/ENG/86D-26

Approved for public release; distribution unlimited

AFIT/GE/ENG/86D-26

FULL POLARIMETRIC NON-SPECULAR SCATTERING OF FLAT PLATE STRUCTURES

THESIS

Presented to the Faculty of the School of Engineering
of the Air Force Institute of Technology
Air University
In Partial Fulfillment of the
Requirements for the Degree of
Master of Science in Electrical Engineering

Jeffrey L. Fath, B.S.E.E.
Second Lieutenant, USAF

December 1986

Acknowledgments

This thesis would not have become a reality without a great deal of assistance from many others. I am very grateful to all of the outstanding people at The Ohio State University ElectroScience Laboratory, especially Dr. Ron Marhefka and Keith Aberegg for their help with the diffraction code, and Dr. Ed Newman for his help with the moment method code. A word of thanks is due to the people of the Avionics Laboratory for their patience and cooperation during the research and writing stages of the thesis. I wish to express my appreciation to my thesis committee, Dr. Alan Lair, Major John Stibravy, and especially Captain Randy Jost for their thoughtful inputs. Finally, I am most deeply indebted to my thesis advisor, Dr. Andy Terzuoli, and my research sponsor, Ed Zelnio, for their divine guidance and inspiration throughout the entire struggle of the thesis.

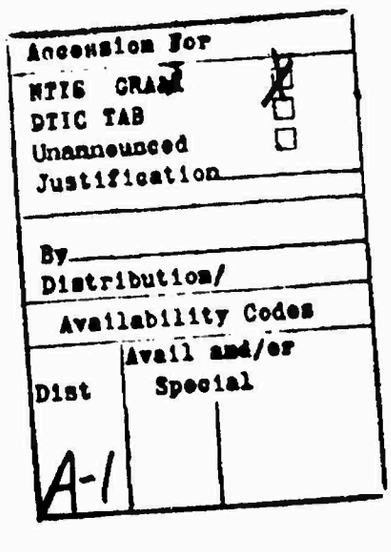

Table of Contents

List of Figures

Abstract

This thesis examined the electromagnetic scattering of a dihedral corner reflector for both monostatic and bistatic source-receiver geometries The full polarization characteristics of the electromagnetic scattering was maintained while the dihedral corner reflector was modeled on and off the principal (horizontal reference) plane. The dihedral corner reflector was composed of two perfectly conducting 9 inch square flat plates joined along a common edge so that they formed an interior angle of 90 degrees. The frequencies of interest included 2, 3, and 10 GHz. The theoretical modeling utilized the Uniform Theory of Diffraction ~~(UTD)~~ and the Method of Moments (MOM). The analysis was performed on a Cray X-MP supercomputer and a VAX 11/785 minicomputer. The results from the models were compared with each other, and with measurements for validation. The measurements were taken on the principal plane for same sense and cross polarization components. The MOM model compared well with measurement for the monostatic and bistatic same sense polarization components. However, differences were noted for the cross polarization component comparison. The MOM model was then extended to off principal plane geometries, which was not measured. A substantial amount of cross polarization scattering was predicted for off principal plane geometries.

FULL POLARIMETRIC NON-SPECULAR SCATTERING OF FLAT PLATE STRUCTURES

I. Introduction

Since the advent of radar, engineers and scientists in electromagnetics have attempted to predict the radar echo area of various targets. The Radar Cross Section (RCS) of a target relates this echo area to the radar. In order to predict the RCS of a target, one needs a thorough understanding of the scattering principles of electromagnetic energy. The basis of all electromagnetic theory begins with Maxwell's equations. However, closed form solutions are available only for simple geometries. Attempts to extend solutions to more complex scattering problems have brought several theories, such as geometrical optics, physical optics, and the theory of diffraction, all of which are based on some approximation.

Present radar systems operate monostatically (colocated transmit and receive antennas) and use same sense polarization (same receive and transmit polarization). This has influenced research to attempt to predict the RCS of targets for monostatic geometries, and same sense polarization. When attempting to model RCS, a target is decomposed into simple shapes such as flat plates, cones, cylinders, etc. The scattering from each of the components is predicted, with the complex, vector sum yielding the total RCS of the target. The scattering from simple shapes is understood for

monostatic geometries, for same sense polarization, and for aspect angles near the specular (point of mirror-like reflection).

Future radars will operate both monostatically and bistatically, and will likely be polarization diverse. These requirements dictate that the modeling techniques for simple shapes be extended. These extensions will be in the area of diffraction terms normally insignificant in geometries and polarizations of current radar systems.

Background

To better prepare the reader to understand the scattering from corner reflectors, a brief historical survey is in order. Corner reflectors are commonly used for monostatic radar enhancement (Kennaugh,1956b). In this application, echo areas much larger than the maximum cross sectional area of the reflector may be obtained.

A dihedral (double bounce) corner reflector is composed of two flat plates connected to form a corner, thus the name corner reflector. Double bounce reflectors do not reverse the rotational sense of a circularly polarized wave, and are therefore desirable for use with circularly polarized radars (Hines,1956a). They respond to circular polarization as well as to linear polarization (Hines,1956b).

A trihedral (triple bounce) corner reflector is composed of three flat plates, joined to form a corner. These operate on the optical principle that an arrangement of three mutually perpendicular reflecting planes will return a triply-reflected ray in the direction of an incident ray (Baeumler,1958). For circularly polarized radars, the sense of the circularly polarized wave is reversed upon reflection from each conducting

wall, so that after 3 reflections, the returning wave is of opposite sense to the incident wave. For this reason, it is not received by the radar, and this is why trihedral corner reflectors are not used with circularly polarized radars (Kennaugh,1956a).

There are several components in analyzing a corner reflector. There are specular and non-specular radar returns. The specular return is due to reflected rays which obey Snell's Law of Reflection, where the angles of incidence and reflection are equal with respect to the surface normal. For the monostatic radar, the reflected ray will be returned in the direction of the incident ray (Baeumler,1958). One finds that the solid angle subtended by the reflected ray is inversely proportional to the square of the corner leg dimensions expressed in wavelengths (Kennaugh,1956b). The non-specular return is due to diffracted rays which result from edges and surface discontinuities. The diffracted rays will scatter in many directions and usually with a change in polarization.

There are several theories attempting to explain the diffraction of electromagnetic energy. The Geometrical Theory of Diffraction (GTD) (Keller,1962) was introduced by Keller as an attempt to predict diffraction. This theory had its share of shortcomings. The Uniform Geometrical Theory of Diffraction (UTD) (Kouyoumjian,1974) was an attempt by Kouyoumjian and Pathak to overcome these shortcomings.

The UTD requires keeping track of all the diffracted rays. Because of the massive bookkeeping task required by UTD, most solutions include only first and second order diffraction terms, which correspond to singly and doubly diffracted rays respectively. The knowledge of solving for higher order terms is available, but because of the massive bookkeeping task required, no general solution includes them. (Marhefka,1984)

Another method of solving RCS problems is the Method of Moments (MOM) (Harrington,1966,1968) as formulated for electromagnetic field theory problems by Harrington. This method uses numerical techniques to solve Maxwell's equations in the integral form, but the electrical size (size in wavelengths) of the object is limited by computer resources.

Problem

This study is to predict the non-specular, electromagnetic scattering of flat plate structures while maintaining polarization diversity, using modeling techniques which handle both monostatic and bistatic geometries.

Scope

While scattering theories are valid for many shapes, this study will only address flat plate structures. In particular the dihedral corner reflector, which is a scatterer normally found on targets of interest, will be analyzed for monostatic and bistatic geometries, aspect angles away from the specular reflection point, and cross polarization. Results of the analysis will be critically compared with measurements of the same scatterer to validate the theoretical development.

Assumptions

The first assumption is that diffraction terms up to the second order are all that are needed to accurately predict the scattering from the geometries considered in this study. Second, the diffraction coefficients used in this study are assumed to be accurate. Finally, the MOM is assumed to accurately predict cross polarization components.

Standards

The experimental data obtained by The Ohio State University ElectroScience Laboratory (OSU-ESL) compact range will be used as the standard to which the theoretical models will be compared. The OSU-ESL compact range is a state of the art measurement facility which can accurately measure electromagnetic energy from 2 to 18 gigahertz (GHz). However, this research will require bistatic cross polarization measurements which OSU-ESL has not previously measured.

General Approach

The problem will be broken into steps according to approach. Step one will be to model the dihedral (double bounce) corner reflector in free space using the UTD. Step two will be to model the dihedral corner reflector in free space with the MOM. Step three will compare the UTD and MOM models with each other. Finally, step four will compare the models to OSU-ESL measurements

The initial attack will be performed with the use of a two dimensional UTD corner reflector computer code developed by Aberegg and Marhefka at OSU-ESL. The code utilizes geometrical optics along with the UTD. The code includes up to third order effects which include single and double diffraction terms.

The next iteration will be to analyze the corner reflector with the Electromagnetic Surface Patch (ESP) Code: Version II - Polygonal Plates and Wires (Newman,1985) developed by Newman at OSU-ESL. The ESP code allows for analysis of both copolarization and cross polarization. The ESP code utilizes the MOM, so it is limited in use by the electrical size of the corner reflector in conjunction with computer resources.

Materials and Equipment

Hardware needed to complete this study includes: a VAX 11/785 computer, a Cray X-MP computer, and a graphics plotter. Software needed includes: the ESP code, the two dimensional UTD corner reflector code, and a plotting routine.

Other Support

Support from Reed and Young of OSU-ESL will be needed in obtaining experimental data to be used for comparison with theoretical results. Support for the use of the computer codes will be provided by Newman, Marhefka, and Aberegg, also of OSU-ESL. Computer support will be provided by the Avionics Laboratory.

Sequence of Presentation

A survey of corner reflector RCS prediction is presented to give the reader a perspective of the electromagnetic scattering for this geometry. In Chapter II, general concepts of electromagnetic wave theory, diffraction theory, and the moment method are presented in relation to the geometries of interest. Chapter III will focus on the analysis of the scatterers using the UTD and MOM codes. Presentation and discussion of the experimental analysis and comparison to measurements will be covered in Chapter IV. Finally Chapter V will present conclusions and recommendations.

Summary

The purpose of this study is to predict the full polarimetric, non-specular scattering from the dihedral corner reflector using the Uniform Geometrical Theory of Diffraction and the Method of Moments.

II. Theoretical Development

Introduction

The thrust of this chapter is to provide the reader with a basic understanding of: 1) basic theory of electromagnetic waves; 2) the Uniform Geometrical Theory of Diffraction (UTD); and 3) the Method of Moments (MOM). The discussion will be limited to those areas applicable to the dihedral corner reflector.

Throughout this writing, all structures are assumed to be perfect electric conductors. The $e^{j\omega t}$ time dependence is assumed and suppressed.

Basic Theory of Electromagnetic Waves

Let us begin this discussion with a definition of terms.

Let

$\mathbf{E}$ = Complex Electric Field Intensity Vector

$\underline{S}_{ij}$ = Complex Scattering Coefficient

$\hat{h}$ = Horizontal Unit Vector

$\hat{v}$ = Vertical Unit Vector

where the bold face indicates a vector, and the underbar indicates a complex value, and the "hat" indicates a unit vector.

An arbitrarily polarized plane wave can be expressed as the sum of two plane waves of orthogonal polarization:

$$\mathbf{E} = \hat{h}E_h + \hat{v}E_v \tag{2-1}$$

where the subscripts refer to the respective orthogonal component, which are complex in general.

The radar cross section (RCS) of an object is an equivalent area defined mathematically by

$$\sigma = \lim_{R\to\infty} 4\pi R^2 \left|\mathbf{E}^s\right|^2 / \left|\mathbf{E}^i\right|^2 \tag{2-2}$$

where

σ = Radar Cross Section

R = Distance Between Radar and Object

$\mathbf{E}^s$ = Scattered Electric Field

$\mathbf{E}^i$ = Incident Electric Field

Current radar systems use the same polarization for both transmit and receive modes. However, the RCS is polarization sensitive and by decomposing the electromagnetic field into the orthogonal components, the RCS can be decomposed into polarization components. The scattered field

can be related to the incident field by the complex scattering coefficients as follows:

$$\begin{aligned} \underline{E}^s_{hh} &= \underline{s}_{hh}\,\underline{E}^i_h \\ \underline{E}^s_{hv} &= \underline{s}_{hv}\,\underline{E}^i_v \\ \underline{E}^s_{vh} &= \underline{s}_{vh}\,\underline{E}^i_h \\ \underline{E}^s_{vv} &= \underline{s}_{vv}\,\underline{E}^i_v \end{aligned} \tag{2-3}$$

or

$$\begin{aligned} \underline{E}^s_h &= \underline{s}_{hh}\,\underline{E}^i_h + \underline{s}_{hv}\,\underline{E}^i_v \\ \underline{E}^s_v &= \underline{s}_{vh}\,\underline{E}^i_h + \underline{s}_{vv}\,\underline{E}^i_v \end{aligned} \tag{2-4}$$

In matrix notation this becomes

$$\begin{bmatrix} \underline{E}^s_h \\ \underline{E}^s_v \end{bmatrix} = \begin{bmatrix} \underline{s}_{hh} & \underline{s}_{hv} \\ \underline{s}_{vh} & \underline{s}_{vv} \end{bmatrix} \begin{bmatrix} \underline{E}^i_h \\ \underline{E}^i_v \end{bmatrix} \tag{2-5}$$

The polarization scattering matrix is now defined by

$$[\underline{S}] = \begin{bmatrix} \underline{s}_{hh} & \underline{s}_{hv} \\ \underline{s}_{vh} & \underline{s}_{vv} \end{bmatrix} \tag{2-6}$$

and the RCS is related to the scattering matrix by (Knott,1985)

$$\sigma_{ij} = \lim_{R\to\infty} 4\,\pi\,R^2\,|\underline{s}_{ij}|^2 \tag{2-7}$$

where the double subscript refers to the polarization of the incident and scattered field, i.e., i = h,v and j = h,v. The cross polarized terms of the

scattering matrix are s_{hv} and s_{vh}, while s_{hh} and s_{vv} are the copolarized terms. The target's horizontal scattered field due to a horizontal incident field is defined by s_{hh}, and the target's vertical scattered field due to a vertical incident field is defined by s_{vv}. The target's depolarization characteristics are defined by s_{hv} and s_{vh}.

The scattering coefficients can be expressed in terms of the incident and scattered electric fields:

$$\begin{aligned} s_{hh} &= \mathbf{E}^s_h / \mathbf{E}^i_h \,\big|\mathbf{E}^i_v=0 \\ s_{hv} &= \mathbf{E}^s_h / \mathbf{E}^i_v \,\big|\mathbf{E}^i_h=0 \\ s_{vh} &= \mathbf{E}^s_v / \mathbf{E}^i_h \,\big|\mathbf{E}^i_v=0 \\ s_{vv} &= \mathbf{E}^s_v / \mathbf{E}^i_v \,\big|\mathbf{E}^i_h=0 \end{aligned} \qquad (2\text{-}8)$$

In general, eight quantities are needed to completely specify the scattering matrix. These eight quantities consist of four magnitudes and four phases. The number can be reduced to seven quantities if one of the phases is used as a reference. If the radar operates monostatically, then $s_{hv} = s_{vh}$, and $[\underline{S}]$ can be specified by five quantities (Knott,1985). Once the scattering matrix is determined, then all of the scattering properties of the target are known for that frequency and target-radar orientation.

For a dihedral corner reflector oriented so that its seam is at an angle α with respect to the horizontal reference (principal) plane, the scattering matrix for the monostatic case is (Cole,1982)

$$[S] = \begin{bmatrix} \cos 2\alpha & \sin 2\alpha \\ \sin 2\alpha & -\cos 2\alpha \end{bmatrix} \qquad (2\text{-}9)$$

The scattered field can then be represented by

$$\begin{bmatrix} \mathbf{E}^s_h \\ \mathbf{E}^s_v \end{bmatrix} = \begin{bmatrix} \cos 2\alpha & \sin 2\alpha \\ \sin 2\alpha & -\cos 2\alpha \end{bmatrix} \begin{bmatrix} \mathbf{E}^i_h \\ \mathbf{E}^i_v \end{bmatrix} \tag{2-10}$$

Uniform Theory of Diffraction

The Uniform Theory of Diffraction (UTD) (Kouyoumjian,1974) developed by Kouyoumjian and Pathak is valid for two and three dimensional edge effects of flat plates with straight edges. Figure 2.1 shows the geometry for the wedge diffraction problem. A source located at $O(s',\phi',z')$ radiates an incident electric field $\mathbf{E}^i(s')$ of arbitrary polarization, which can have a plane, cylindrical, or spherical wavefront. The diffraction of the incident field occurs at the point Q_E (or points in the case of a plane wave) which is unique for a given source and observation location. Kouyoumjian and Pathak have shown that the calculation of the diffracted field at the observation point $P(s,\phi,z)$ can be simplified if a fixed coordinate system centered at Q_E is used (Kouyoumjian,1974). The diffraction of the incident ray forms a cone of diffracted rays whose axis is the edge with a cone angle equal to the incident angle, i.e. $\beta_0 = \beta'_0$.

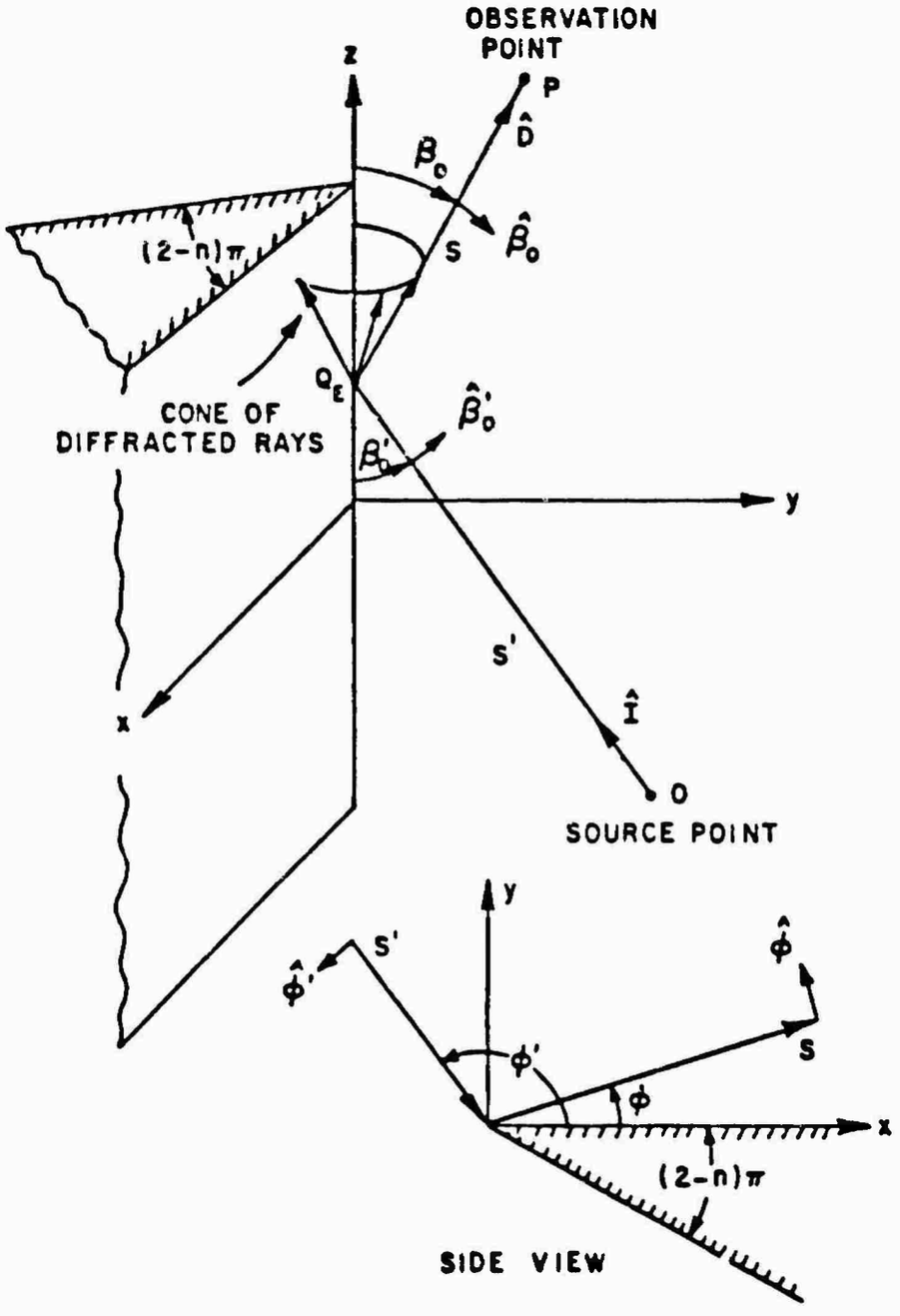

FIGURE 2-1. GEOMETRY FOR THREE-DIMENSIONAL WEDGE DIFFRACTION PROBLEM

The set of orthogonal unit vectors associated with the ray fixed coordinate system are defined as follows:

$$\hat{\imath} = \hat{\beta}'_o \times \hat{\phi}'$$

$$\hat{D} = \hat{\beta}_o \times \hat{\phi}$$

where $\hat{\imath}$ is the incident propagation direction unit vector, and $\hat{D}$ is the diffraction propagation direction unit vector. The diffracted field is given by (Kouyoumjian,1974)

$$\mathbf{E}^d(s) \sim \mathbf{E}^i(Q_E) \cdot \langle \underline{D}_E(\hat{D},\hat{\imath}) \rangle A(s)\, e^{-jks} \tag{2-11}$$

where the diffraction dyadic is given by

$$\langle \underline{D}_E(\hat{D},\hat{\imath}) \rangle = -\hat{\beta}'_o\hat{\beta}_o\underline{D}_s - \hat{\phi}'\hat{\phi}\underline{D}_h \tag{2-12}$$

and the terms of the diffraction dyadic are

$$\begin{aligned} D_{s,h}(L,\phi,\phi',\beta_o) = {} & [\,(-e^{-j\pi/4}) / (2n\,(2\pi k)^{1/2}\sin\beta_o)\,] \\ & \times \{\cot[(\pi+\beta^-)/(2n)]\, F[kLa^+(\beta^-)] \\ & + \cot[(\pi-\beta^-)/(2n)]\, F[kLa^-(\beta^-)] \\ & \mp (\cot[(\pi+\beta^+)/(2n)]\, F[kLa^+(\beta^+)] \\ & + \cot[(\pi-\beta^+)/(2n)]\, F[kLa^-(\beta^+)])\} \end{aligned} \tag{2-13}$$

where

L = distance parameter dependent on wavefront

k = wavenumber (2π / wavelength)

$\beta^{\pm}$ = sum/difference angle of $\hat{D}$ and $\hat{I}$ as measured in the x-y plane

β_o = angle of reflection as measured from the z axis

A(s) = spread factor of wavefront

n = wedge angle number

and

$$a^{\pm}(\beta) = 2 \cos^2 [\{ 2n\pi N^{\pm} - (\beta) \} / 2] \qquad (2\text{-}14)$$

where $N^{\pm}$ are the integers which most nearly satisfy the equations

$$2n\pi N^{+} - (\beta) = \pi$$

and

$$2n\pi N^{-} - (\beta) = -\pi$$

with

$$\beta = \beta^{\pm} = \phi \pm \phi'$$

$\mathbf{F}$ is a transition function that was included by Kouyoumjian and Pathak to improve the diffracted field solution in the transition regions of the incident and reflection shadow boundaries. $\mathbf{F}(x)$ is defined by

$$\mathbf{F}(x) = 2j \left| x^{1/2} \right| e^{jx} \int e^{-jt^2} \, dt \qquad (2\text{-}15)$$

The magnitude and phase of $F(x)$ are plotted in Figure 2-2. Kouyoumjian and Pathak used the following approximation for small arguments ($x<0.3$)

$$F(x) \sim [(\pi x)^{1/2} - 2x e^{j\pi/4} - (2/3)x^2 e^{-j\pi/4}] e^{j(\pi/4+x)} \qquad (2\text{-}16)$$

and for large arguments ($x>5.5$)

$$F(x) \sim 1 + j/(2x) - 3/(4x^2) - j15/(8x^3) + 75/(16x^4) \qquad (2\text{-}17)$$

If n=2, then the wedge reduces to a half plane and the diffraction coefficient reduces to

$$\begin{aligned} D_{s,h}(L,\phi,\phi',\beta_o) = {} & [(-e^{-j\pi/4})/(2\{2\pi k\}^{1/2}\sin\beta_o)] \\ & x [F\{kLa(\beta^-)\}/\cos(\beta^-/2) \\ & \mp F\{kLa(\beta^+)\}/\cos(\beta^+/2)] \end{aligned} \qquad (2\text{-}18)$$

Another special case of the diffraction coefficients occurs when the source and receiver are in the far field of the wedge, so that $F(x)$ is approximately equal to 1. For this case the diffraction coefficients reduce to Keller's diffraction coefficients (Keller, 1962):

$$\begin{aligned} D_{s,h}(L,\phi,\phi',\beta_o) = {} & [(-e^{-j\pi/4})/(2\{2\pi k\}^{1/2}\sin\beta_o)] \\ & x [\cot(\{\pi+\beta^-\}/\{2n\}) + \cot(\{\pi-\beta^-\}/\{2n\}) \\ & \mp \{\cot(\{\pi+\beta^+\}/\{2n\}) + \cot(\{\pi-\beta^+\}/\{2n\})\}] \end{aligned} \qquad (2\text{-}19)$$

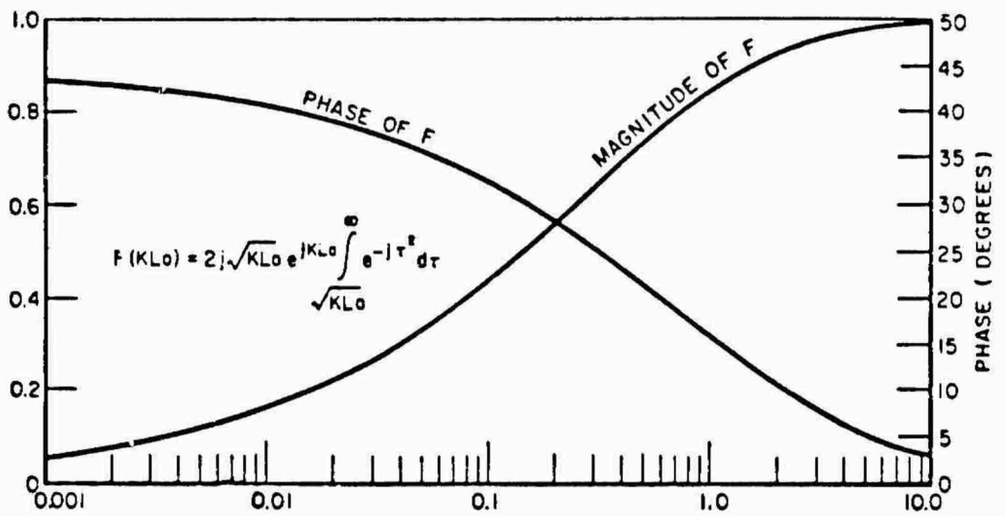

FIGURE 2-2. TRANSITION FUNCTION

The diffracted fields can be written in matrix form as

$$\begin{bmatrix} \mathbf{E}^d_{\beta o}(s) \\ \\ \mathbf{E}^d_{\phi}(s) \end{bmatrix} = \begin{bmatrix} -\underline{D}_s & 0 \\ \\ 0 & -\underline{D}_h \end{bmatrix} \begin{bmatrix} \mathbf{E}^i_{\beta' o}(Q_E) \\ \\ \mathbf{E}^i_{\phi'}(Q_E) \end{bmatrix} A(s)\, e^{-jks} \quad (2\text{-}20)$$

The diffraction dyadic matrix is diagonal because of the ray fixed coordinate system employed. The subscripts s and h refer to the soft and hard boundary conditions respectively. The soft diffraction coefficient, $\underline{\mathbf{D}}_s$, uses the soft boundary condition (E field component parallel to the edge):

$$\mathbf{E}_{\parallel} \big|_{\text{wedge}} = 0 \quad (2\text{-}21)$$

and the hard diffraction coefficient, $\underline{\mathbf{D}}_h$, uses the hard boundary condition (E field component perpendicular to the edge):

$$\partial \mathbf{E}_{\perp} / \partial n \big|_{\text{wedge}} = 0 \quad (2\text{-}22)$$

The spread factor, A(s), and the distance parameter, L, are dependent on the type of incident wave such that

$$A(s) = \begin{cases} (s)^{-1/2} & \text{plane, cylindrical, \& conical} \\ & \text{wave incidence} \\ (s' / (s\,(s+s'))^{1/2} & \text{spherical wave incidence} \end{cases} \qquad (2\text{-}23)$$

$$L = \begin{cases} s\ \sin^2\beta_0 & \text{plane wave incidence} \\ s\ s' / (s+s') & \text{cylindrical wave incidence} \\ ss'\ (\sin^2\beta_0) / (s+s') & \text{conical \& spherical wave incidence} \end{cases} \qquad (2\text{-}24)$$

The Method of Moments

The Method of Moments (MOM) is a general procedure for solving linear equations (Harrington,1966,1968). The MOM starts with a general, inhomogeneous equation:

$$L(f) = g \qquad (2\text{-}25)$$

where L is an arbitrary, linear operator, g is the known, and f is the unknown to solve. Begin by letting f be represented by a series solution of f_n, where f_n is in the domain of the operator L:

$$f = \sum_n a_n f_n \qquad (2\text{-}26)$$

where a_n are the constant coefficients to find. The functions f_n are called the expansion or basis functions. Usually an infinite summation of a complete set of orthogonal expansion functions is needed for an exact

solution, but only a finite summation is needed for an approximate solution.

Now substitute Equation (2-26) into (2-25) to obtain

$$L\left(\sum_n a_n f_n\right) = g \tag{2-27}$$

and use the linearity property of L to get

$$\sum_n a_n L(f_n) = g \tag{2-28}$$

Next, introduce an inner product $\langle x,y \rangle$, which is a scalar defined by

$$\langle x,y \rangle = \int_0^1 x(t)\, y(t)\, dt \tag{2-29}$$

A set of weighting or testing functions w_m must be defined in the range of L. Take the inner product of Equation (2-28) with w_m to get

$$\sum_n a_n \langle w_m, L(f_n) \rangle = \langle w_m, g \rangle \tag{2-30}$$

With m = 1,2,3,···, a system of equations can now be written in matrix form:

$$[\, l_{mn} \,]\{\, a_n \,] = [\, g_m \,] \tag{2-31}$$

where

$$[\, l_{mn} \,] = \begin{bmatrix} \langle w_1, L(f_1) \rangle & \langle w_1, L(f_2) \rangle & \cdots \\ \langle w_2, L(f_1) \rangle & \langle w_2, L(f_2) \rangle & \cdots \\ \cdots & \cdots & \cdots \end{bmatrix} \tag{2-32}$$

$$[a_n] = \begin{bmatrix} a_1 \\ a_2 \\ \cdot \\ \cdot \\ \cdot \end{bmatrix} \qquad [g_m] = \begin{bmatrix} \langle w_1, g \rangle \\ \langle w_2, g \rangle \\ \cdot \\ \cdot \\ \cdot \end{bmatrix} \tag{2-33}$$

As long as the inverse of $[l_{mn}]$ exists, then a_n is given by

$$[a_n] = [l_{nm}]^{-1} [g_m] \tag{2-34}$$

Representing f_n as a matrix of functions

$$[f_n] = [f_1 \; f_2 \; f_3 \cdots] \tag{2-35}$$

the solution of f may be written as

$$f = [f_n][a_n] = [f_n][l_{nm}]^{-1} [g_m] \tag{2-36}$$

This solution may be approximate or exact, depending on the choice of the expansion (basis) and testing (weight) functions, f_n and w_m respectively. A special case called the Galerkin's Method occurs when $f_n = w_n$.

Next, applying the MOM to an electromagnetic field problem, start with Maxwell's equations in the time harmonic form:

$$\nabla \times \mathbf{E} = -j\omega\mu\mathbf{H}$$

$$\nabla \times \mathbf{H} = j\omega\varepsilon\mathbf{E} + \mathbf{J} \tag{2-37}$$

where $\mathbf{E}$ is the electric field intensity, $\mathbf{H}$ the magnetic field intensity, and $\mathbf{J}$ the electric current density. Combining the above equations into a single equation for $\mathbf{E}$ yields

$$-(j\omega)^{-1}\nabla \times (\mu^{-1}\nabla \times \mathbf{E}) - j\omega\varepsilon\mathbf{E} = \mathbf{J} \tag{2-38}$$

In the form of the MOM operator notation, this becomes

$$-L(\mathbf{E}) = \mathbf{J} \tag{2-39}$$

Consider an arbitrarily shaped scatterer in a homogeneous medium. An impressed source ($\mathbf{J}^i$, $\mathbf{M}^i$) radiates the fields ($\mathbf{E}^i$, $\mathbf{H}^i$) in free space and the fields ($\mathbf{E}^T$, $\mathbf{H}^T$) in the presence of the scatterer. For a perfect electric conductor, surface currents $\mathbf{J}_s$ are induced on the surface of the scatterer, which produce the scattered field $\mathbf{E}^s$. Apply Equation (2-39) to the scatterer to get

$$-L(\mathbf{E}^s) = \mathbf{J}_s \tag{2-40}$$

Applying the inverse operator to both sides yields the potential integral solution to Equation (2-40):

$$-\mathbf{E}^s = L^{-1}(\mathbf{J}_s) = -j\omega\mathbf{A}^s - \nabla\Phi^s \tag{2-41}$$

where

$$\mathbf{A}^s(\mathbf{r}) = \mu \iiint \mathbf{J}_s(\mathbf{r}')\,(4\pi|\mathbf{r}-\mathbf{r}'|)^{-1}\, e^{-jk|\mathbf{r}-\mathbf{r}'|}\, dv'$$

$$\Phi^s(\mathbf{r}) = \varepsilon^{-1} \iiint \rho_s(\mathbf{r}')\,(4\pi|\mathbf{r}-\mathbf{r}'|)^{-1}\, e^{-jk|\mathbf{r}-\mathbf{r}'|}\, dv'$$

$$\rho_s = -(j\omega)^{-1}\,\nabla\cdot\mathbf{J}_s$$

On the surface of the scatterer, the boundary conditions on the electric field are such that the tangential component must vanish:

$$\hat{n} \times \mathbf{E}^T = \hat{n} \times (\mathbf{E}^i + \mathbf{E}^s) = 0 \tag{2-42}$$

Thus

$$\mathbf{E}^i{}_{tan} = -\mathbf{E}^s{}_{tan} \tag{2-43}$$

where the subscript "tan" means the tangential component of the electric field. Thus, Equation (2-41) becomes

$$\mathbf{E}^i{}_{tan} = L^{-1}(\mathbf{J}_s) \tag{2-44}$$

To continue along the lines of the MOM solution, a suitable inner product must be chosen. For electromagnetic field problems, a suitable inner product is

$$\langle \mathbf{E}, \mathbf{J} \rangle = \iiint \mathbf{E} \cdot \mathbf{J} \, dv' \tag{2-45}$$

which is the definition of reaction (Harrington,1966,1968). Equation (2-45) can be expressed as an integral over the surface of the scatterer since $\mathbf{J}$ is the surface current density and $\mathbf{E}$ is limited to the tangential component on the surface.

The next step is to expand the surface current density $\mathbf{J}_s$ in terms of N expansion (basis) functions $\mathbf{J}_n$.

$$\mathbf{J}_s = \sum_{1}^{N} I_n \mathbf{J}_n \tag{2-46}$$

Substitute Equation (2-46) into Equation (2-44) to get

$$L^{-1} \left(\sum_{1}^{N} I_n \mathbf{J}_n \right) = \mathbf{E}^i{}_{tan} \tag{2-47}$$

and since L is a linear operator, Equation (2-47) becomes

$$\sum_{1}^{N} I_n L^{-1} (\mathbf{J}_n) = \mathbf{E}^i{}_{tan} \tag{2-48}$$

Next choose a set of testing (weight) functions $\mathbf{W}_n$ which are also tangential to the surface. Apply the inner product defined in Equation (2-45) to Equation (2-48) and $\mathbf{W}_n$ to obtain

$$\sum_{1}^{N} I_n \langle \mathbf{W}_m, L^{-1} (\mathbf{J}_n) \rangle = \langle \mathbf{W}_m, \mathbf{E}^i{}_{tan} \rangle \tag{2-49}$$

Now the system of equations can be represented in matrix notation:

$$[\,Z_{mn}\,][\,I_n\,] = [\,\underline{V}_m\,] \tag{2-50}$$

where

$$[\,I_n\,] = \begin{bmatrix} I_1 \\ I_2 \\ \cdot \\ \cdot \\ \cdot \end{bmatrix} \qquad [\,\underline{V}_m\,] = \begin{bmatrix} \langle \underline{W}_1, \underline{E}^i \rangle \\ \langle \underline{W}_2, \underline{E}^i \rangle \\ \cdot \\ \cdot \\ \cdot \end{bmatrix}$$

$$[\,Z_{mn}\,] = \begin{bmatrix} \langle \underline{W}_1, L^{-1}(\underline{J}_1) \rangle & \langle \underline{W}_1, L^{-1}(\underline{J}_2) \rangle & \cdots \\ \langle \underline{W}_2, L^{-1}(\underline{J}_1) \rangle & \langle \underline{W}_2, L^{-1}(\underline{J}_2) \rangle & \cdots \\ \cdots & \cdots & \cdots \end{bmatrix} \tag{2-51}$$

Solving for $[\,I_n\,]$ one obtains

$$[\,I_n\,] = [\,Z_{nm}\,]^{-1}\,[\,\underline{V}_m\,] \tag{2-52}$$

and

$$J = [\,\underline{J}_n\,][\,I_n\,] = [\,\underline{J}_n\,][\,Z_{nm}\,]^{-1}\,[\,\underline{V}_m\,] \tag{2-53}$$

where the elements of the impedance and excitation matrix are given by

$$\underline{Z}_{mn} = - \iint \mathbf{E}_m \cdot \mathbf{J}_n \, ds$$

$$\underline{V}_m = \iiint \mathbf{J}_m \cdot \mathbf{E}^i \, dv \qquad (2\text{-}54)$$

$\underline{Z}_{mn}$ is integrated over the surface of the n-th expansion mode, and is called the mutual impedance between modes m and n. $\underline{V}_m$ is integrated over the volume occupied by the source ($\mathbf{J}^i$, $\mathbf{M}^i$), and is called the modal excitation voltage.

III. Analysis

Choosing the Approach

During the initial discussions with Zeinio, the sponsor of this research, the approach to attacking the problem of the dihedral corner reflector could have taken several paths. The sponsor's contract for the indoor measurements was with The Ohio State University ElectroScience Laboratory (OSU-ESL) in Columbus Ohio, so one obvious approach was to use the Uniform Geometrical Theory of Diffraction (UTD), which was greatly advanced by OSU. For comparison and validation purposes, another approach should be pursued to check against measurements.

When used properly, the Method of Moments (MOM) approaches the exact solution of Maxwell's integral equations. Therefore, the MOM was thought of as the best approach to compare with the UTD results and the measurements. The problem with MOM is that as the object modeled becomes larger in electrical size (size in wavelengths) the amount of computer memory required increases, and the CPU time increases substantially. Thus, the computer resources limit the size of an object which could be modeled by the MOM. Much research has been done on modifying the MOM to handle larger problems. From this research several special techniques have emerged which could solve MOM problems faster and handle larger electrical sizes.

Since a 9 inch dihedral corner reflector at 10 gigahertz (GHz) is 116 square wavelengths in electrical size, an alternative to the original MOM approach should be investigated. Even at 3 GHz the dihedral is 10.5 square

wavelengths, which would be considered a large problem for MOM. Should one of the special MOM techniques be pursued or should an alternative solution be pursued?

After a thorough search of the literature, one technique seemed to be the most promising for the problem at hand. The Spectral Domain Approach, also called the Spectral Theory of Diffraction (STD) (Mittra,1972), was developed by Mittra and Li at the University of Illinois at Urbana-Champaign. The STD uses a UTD solution as an initial guess, and then through an iterative technique comes to a final solution.

The Southeastern Center for Electrical Engineering Education (SCEEE) sponsored a short course on RCS computational techniques at the University of Illinois at Urbana-Champaign, and Mittra was the coordinator of the short course. At the short course, the problem of the dihedral corner reflector was presented to Mittra. The STD has been used to obtain results on a square flat plate and on an infinite rectangular cylinder, both of which are related to the dihedral corner reflector problem. However, Mittra suggested that the STD would be too difficult to apply to the dihedral problem, and that there were other techniques which would be better suited for the dihedral.

Mittra proposed using a special technique with the MOM. His suggestion involved using the Physical Optics (PO) approximation of the surface current as an entire domain expansion (basis) function on the portions of the dihedral surface which were sufficiently far enough away from the edges. On the regions near the edges, the technique of subsectional basis functions could then be used with the MOM.

After the investigation of the methods available to attack the dihedral corner reflector problem, another factor had to be considered--time. Because of the limited amount of time alloted to complete the research, an approach or approaches had to be selected on the merit that they could be completed. Aberegg and Marhefka at OSU had been working on a computer code utilizing the UTD to solve a two dimensional dihedral corner reflector. This seemed to be the logical choice for doing the UTD analysis on the corner reflector. Next, the alternative method needed to be chosen.

With the knowledge that a Cray supercomputer was available for computation, a general MOM solution was sought after which could be modified for the dihedral. The supercomputer would alleviate the problem of the slowness of the MOM solution. A general purpose MOM code, the Electromagnetic Surface Patch (ESP) Code: Version II - Polygonal Plates and Wires (Newman,1985), was found through the help of the people at OSU. The ESP code is based on the Electric Field Integral Equation (EFIE), so it was ideal for open structures such as the dihedral corner reflector.

Now that a UTD code and a MOM code had been obtained, the attack on the dihedral corner reflector problem could begin. The plan was to run the UTD corner reflector code on a VAX 11/785 computer, and since the code was developed (and still being developed at the time of this writing) on a VAX 11/780 computer this should have been no problem. The ESP code was also developed on the VAX 11/780 computer, but the intention of running the code on the Cray X-MP 12 Serial 315/75 computer opened up the potential trouble area of Fortran compiler ambiguities.

Implementation of the MOM Code

Because of the potential trouble area with the Fortran compilers, the implementation of the ESP code on the Cray was the first approach tried on the dihedral corner reflector. The Cray needs another computer connected to it as a front end for obtaining interactive access. This front end computer was also a VAX 11/785. After the ESP code was uploaded from the front end VAX, the testing of the ESP code on the Cray began.

The first thing the Cray didn't recognize was the use of special control characters in the code which performed various functions such as tabbing, line feeding, and form feeding. Some of the control characters were removed globally with the VAX editor, while others had to be removed on a line by line basis. Considering the fact that the ESP code was over 7800 lines in length, stripping all of the special control characters was no quick and easy task. Once the special control characters were removed, more Fortran compiler ambiguities became apparent. The most frequently encountered difference was in the use of input/output (I/O) statements, such as "open" and "close" statements. After modifying the code to the format required by the Cray, it finally compiled without errors.

The code operated with an input parameter file which needed to be assigned to the logical device unit number "5". This unit number was then opened by the ESP code and the program read the input parameter file. After some final fine tuning, the ESP code was ready to be tested on the Cray. Starting with input parameters provided by Newman, the author of the ESP code, the version of the code on the Cray could be validated with known results. The Cray performed superbly in calculating the test run

approximately 20 times faster than the VAX. How well would the Cray perform on the dihedral corner reflector at 3 GHz?

As stated previously, the dihedral at 3 GHz is approximately 10.5 square wavelengths electrically. Sampling 4 times per wavelength yielded approximately 24 modes per square wavelength. Including overlap modes, this gave a total of 261 modes for which to solve. The ESP code was originally dimensioned to allow up to 500 total modes, so half of the total was used. For better accuracy, sampling around 8 times per wavelength resulted in 112 modes per square wavelength for a total of 1194 modes, which was more than double the dimensions in the ESP code, so the dimensions of the arrays in the code needed increasing.

As a first attempt, the arrays were increased to 2000, four times the original value. The code compiled without problems, but during execution the Cray aborted the run with an indication that more memory was requested than available. After consultation with the Cray Research analysts, the conclusion was drawn that the Cray couldn't handle the code with the arrays dimensioned that large. The Cray X-MP 12 Serial 315/75 has 16 megabytes (MB) of main memory, but each word is 8 bytes long so the machine has a total of 2 mega words (MW) of main memory. The code itself used about 30 kilowords (KW), and the Cray Operating System (COS) consumed about 200 KW of memory, leaving 1.77 MW for the variables in the code.

After careful examination of the code and consultation with Newman, a dimension of about 1000 appeared to be the largest the Cray could handle. With the code dimensioned to allow arrays of up to 1000 elements, the code compiled and executed without trouble. Thus, the

maximum the dihedral could be sampled at 3 GHz was 7 times per wavelength.

At 10 GHz and with the arrays dimensioned at 1000, the maximum the dihedral could be sampled would have been only two times per wavelength! Not nearly enough even for an approximate result, and an accurate answer was desired. At this point, it became very apparent that the Cray was not the solution to running a large MOM program. The Cray has the computational speed required, but lacks the required main memory for a large matrix problem. The Cray analysts were aware of the memory problem and had plans of upgrading the memory to 48 MB (3 times the current memory) in May of 1987. However, this planned memory increase didn't help the current problem, and would not be implemented in time for this thesis.

Now there was a big problem--how to run the ESP code for larger objects. Turning to the only other computer at hand, the VAX 11/785, the version of the ESP code with the 2000 dimensioned arrays was compiled, but couldn't be linked because of a lack of virtual address space. The VAX system operator increased the virtual address space, but once again the program wouldn't link due to the pagefile quota being exceeded. After the pagefile was increased by the system operator, the program linked without any trouble, but upon execution of the program the VAX aborted the run due to the memory being full. The VAX system message and error recovery documentation was very useful, and led to a solution to increase the memory that any single job could use. This was defined by the working set default (WSdef) and extent (WSext) in both the user authorization file (UAF) and the system generation utility (SYSGEN) With all the changes

made to the operating system, the program finally executed for the dihedral at 3 GHz with 7 samples per wavelength.

With all the work required to run the program at 3 GHz, what would it take to get the program to run at 10 GHz? Again, the virtual address space, page file quota, and the working set parameters were increased. The dimensions in the ESP code were now increased to 4000, allowing the dihedral to be analyzed at 10 GHz with a sampling rate of 4 times per wavelength, the minimum needed for engineering accuracy. Again, the VAX aborted the job because of a lack of memory. This time it was thought that the Digital Electronic Corporation (DEC), the makers of the VAX, should be called in on this problem.

The DEC analyst for the VAX suggested configuring the system to allow the user full access of the computer's resources. Using a backup of the operating system, the system disk was configured to the specifications the VAX analyst suggested. This time the program began to execute. To the casual observer, it appeared that the VAX was operating normally. However, the next morning the system slowed down to a standstill, and the system had to be powered down and rebooted. Since the trouble didn't appear to begin until other users were on the system, and knowing that the program was allowed the entire system's resources, it seemed possible that the program might run over the weekend when there were no other users with which to compete.

With the anticipation that the program would execute, it was again submitted. After about 18 hours of CPU time, it became apparent that the system had slowed down to a standstill once again. But a message on the operator's console provided insight as to why the program wouldn't run.

Since the VAX is a virtual addressing computer, it pages in and out of the main memory to a disk file called the pagefile. The problem was that the pagefile was not large enough to handle all the pages created by the program. This problem was alleviated by increasing the size of the pagefile to approximately four times the size of the original pagefile. This allowed the program space to page in and out of the main memory. The ESP code finally started executing without signs of trouble. After 12 days elapsed, the VAX had to be powered down due to a problem with the air conditioning system. At this point, the code had used approximately 120 hours of CPU time, and had completed 77% of the 360 total field points. Because of the dihedral's symmetry in the monostatic case, the remaining points could be extrapolated.

Implementation of the UTD Code

When it became apparent that there would be problems running the ESP code, the analysis of the dihedral corner reflector was started with the UTD two dimensional corner reflector code developed by Aberegg and Marhefka at OSU. The code included first, second, and third order effects,

which included single, and double diffraction. Thus, the code included the following terms:

single diffracted (D)

diffracted-reflected and reflected-diffracted (DR,RD)

reflected-diffracted-reflected (RDR)

diffracted-double reflected and double reflected-diffracted (DRR, RRD)

double diffracted (DD)

diffracted-reflected-diffracted (DRD)

double diffracted-reflected and reflected-double diffracted (DDR, RDD)

The code was a two dimensional model, so it couldn't predict cross polarization components or off principal plane scattering.

A very strong advantage of the UTD solution is the speed of computation and the small amount of computer resources required. Since the diffraction coefficients consist of little more than a combination of trigonometric functions, solutions are easily and speedily obtained. This allowed the dihedral to be analyzed at 10 GHz, where the ESP code had a difficult time doing because of computer limitations. Another feature of the UTD analysis is the RCS is broken up into the individual components of the scattering interactions, thus bringing insight into the physical phenomena.

Unlike the ESP code, the UTD code ran interactively, with the user entering responses after the code prompted for an input. The program first asks for the width of the strips and the flare angle between them. Since the code was a two dimensional model, the dihedral corner reflector only had width as a variable, with the length being infinite. The code then prompts for either a monostatic or bistatic case. If the run is for a bistatic

case, then it prompts for the bistatic angle. The next 7 prompts are for the scattering terms the code is to include in the run. Lastly, the code prompts for either the soft or hard boundary condition. Even if all the scattering effects were included, the code only took a few seconds to complete, unlike the MOM code which took hours.

The UTD corner reflector code worked well. The only problem areas occurred when the observation point was on the diffraction shadow boundary (SB) or reflection shadow boundary(RB). The DD component tended toward infinity rather than approaching the proper limit. A uniform double diffraction solution had only recently been solved by Tiberio and Kouyoumjian (Aberegg,1985) and was not yet implemented in this code.

The UTD corner reflector code did not experience any problems of the magnitude that the ESP code experienced. The ESP code presented quite a demand for computer system resources, and as a result required more time and effort in running. However, the ESP solved for both cross and same sense polarization, so it was preferred when the object was not electrically large.

IV. Results and Discussion

Introduction

In this chapter the results of the UTD two dimensional corner reflector code and the ESP code will be presented and compared to measurements taken at The Ohio State University ElectroScience Laboratory (OSU-ESL). The geometry of the dihedral corner reflector is shown in Figure 4-1. The dihedral consists of two 9 by 9 inch square flat plates joined to form an interior angle of 90 degrees. The plates' material is assumed to be perfectly conducting.

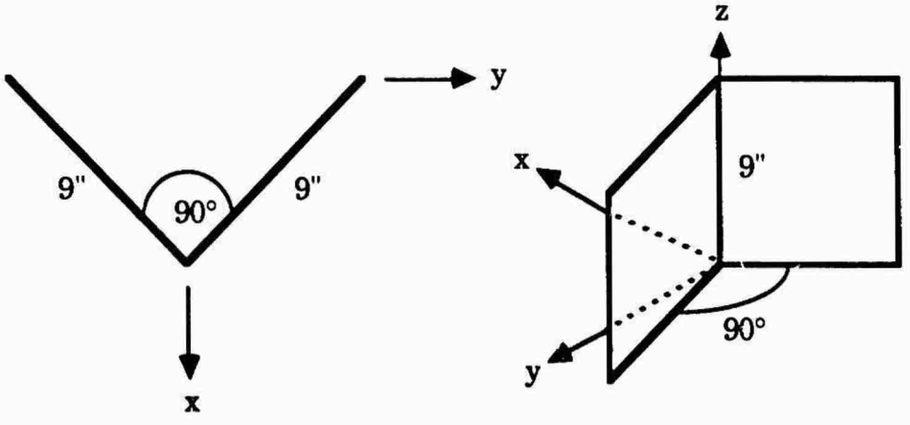

Figure 4.1 Dihedral Corner Reflector

The dihedral corner reflector was analyzed at 2, 3, and 10 GHz using the UTD two dimensional corner reflector code. Because the UTD is a high frequency approximation, the accuracy of the results is expected to degrade

as the the frequency is decreased. The ESP moment method code was used to analyze the dihedral at 2 and 3 GHz with the possibility of obtaining results at 10 GHz. The accuracy of the ESP code does not depend on frequency, but rather on the wavelength sampling rate. However, as the frequency is increased the matrix in the ESP code becomes large which forces the sampling rate to be lowered, thus affecting the accuracy.

The dihedral was modeled for both monostatic and 90° bistatic geometries. The dihedral was also modeled off the principal plane with the ESP code. Recall that the UTD cannot model the dihedral off the principal plane because the model is two dimensional. Cross polarization could only be modeled with the ESP code, because the UTD code is two dimensional.

ESP Code Solutions

At what wavelength sampling rate does the ESP code's solution converge when analyzing the dihedral? What testing function should be used to achieve the most accurate results? What are the tradeoffs between the two testing functions in terms of accuracy, computation speed, and computer storage? These questions need to be considered when using the ESP code to model the scattering from any target.

The solution the ESP code generates becomes more accurate as the sampling rate is increased per wavelength. Figure 4-2 shows the monostatic RCS of the dihedral at 3 GHz for theta in theta out polarization (soft boundary condition on the electric field), and for phi in phi out polarization (hard boundary condition on the electric field). The graph shows the comparison between filament testing and full surface patch testing with a 0.25 wavelength patch (4 samples per wavelength). For theta

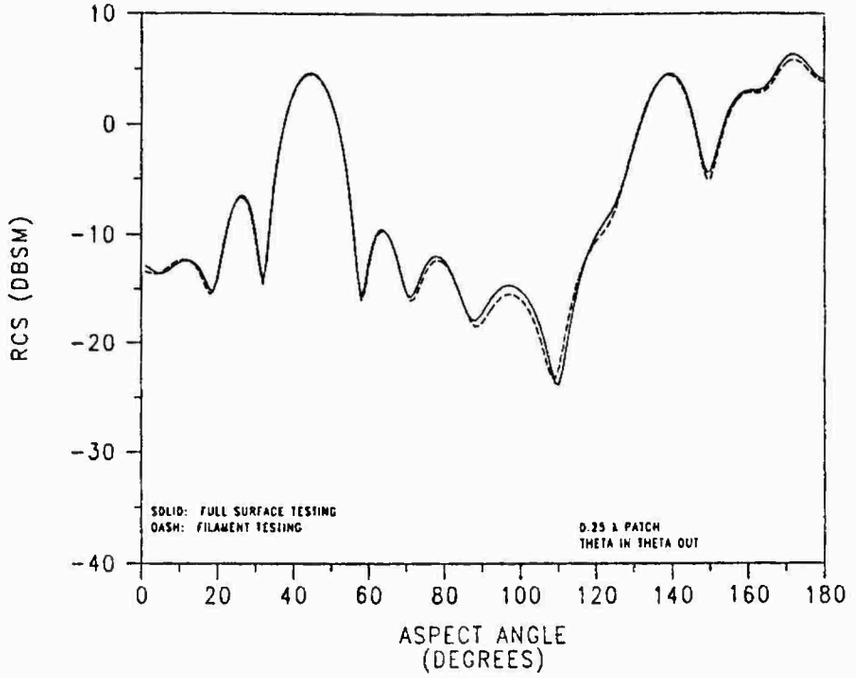

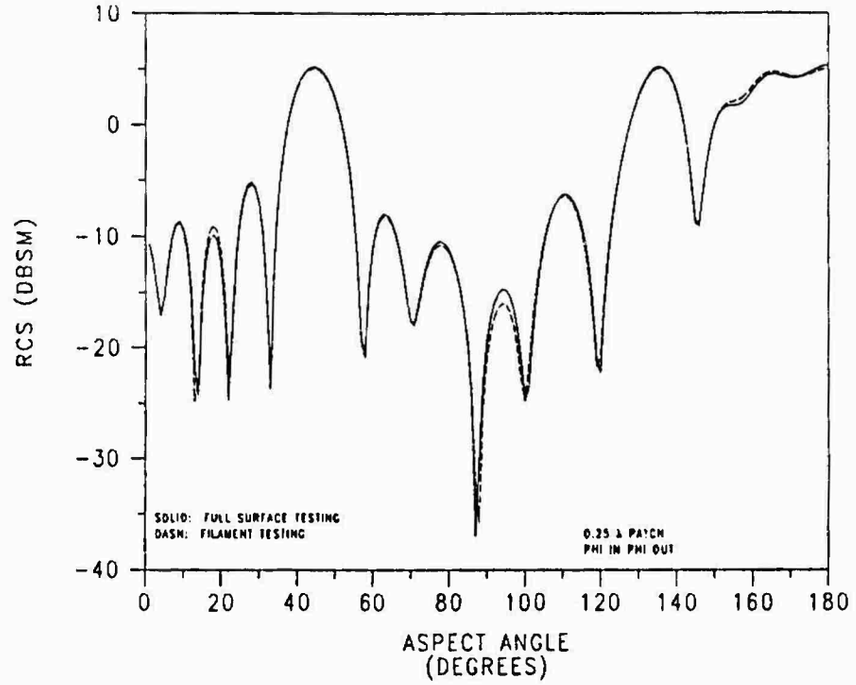

FIGURE 4-2. MONOSTATIC RCS OF 9" DIHEDRAL AT 3 GHZ
FILAMENT VERSUS FULL SURFACE TESTING COMPARISON

polarization, the two methods differ slightly in the 0° to 20°, 70° to 130°, and 150° to 180° regions. The most significant discrepancy occurs around 110° where the location of the nulls differ. Despite the minor differences the two methods show excellent agreement.

Figure 4-3 compares the two testing methods with a 0.20 wavelength patch (5 samples per wavelength). There is only slight disagreement between the two methods in the same aspect angle regions, but the differences are decreasing. In Figure 4-4 the two methods again show slight disagreement, but are converging to the same result with patch size of 0.15 wavelengths (6.67 samples per wavelength). The most significant difference occurs in the 90° to 100° region of the phi in phi out pattern, but differs by 2 dB at most. This gives reasonable confidence in the two separate testing methods as they both tend toward the same result.

Figure 4-5 shows the comparison between 0.15, 0.20, and 0.25 wavelength patches for filament testing. and the largest difference is at 110° for theta in theta out. Elsewhere there is good agreement between the sampling rates for filament testing. Figure 4-6 shows the same comparison for full surface testing, For theta in theta out, the worst agreement occurs at 110°, a difference of almost 5 dB. But elsewhere only small differences exist between the sampling rates giving confidence in the results, with the 0.15 wavelength patch giving the most confidence.

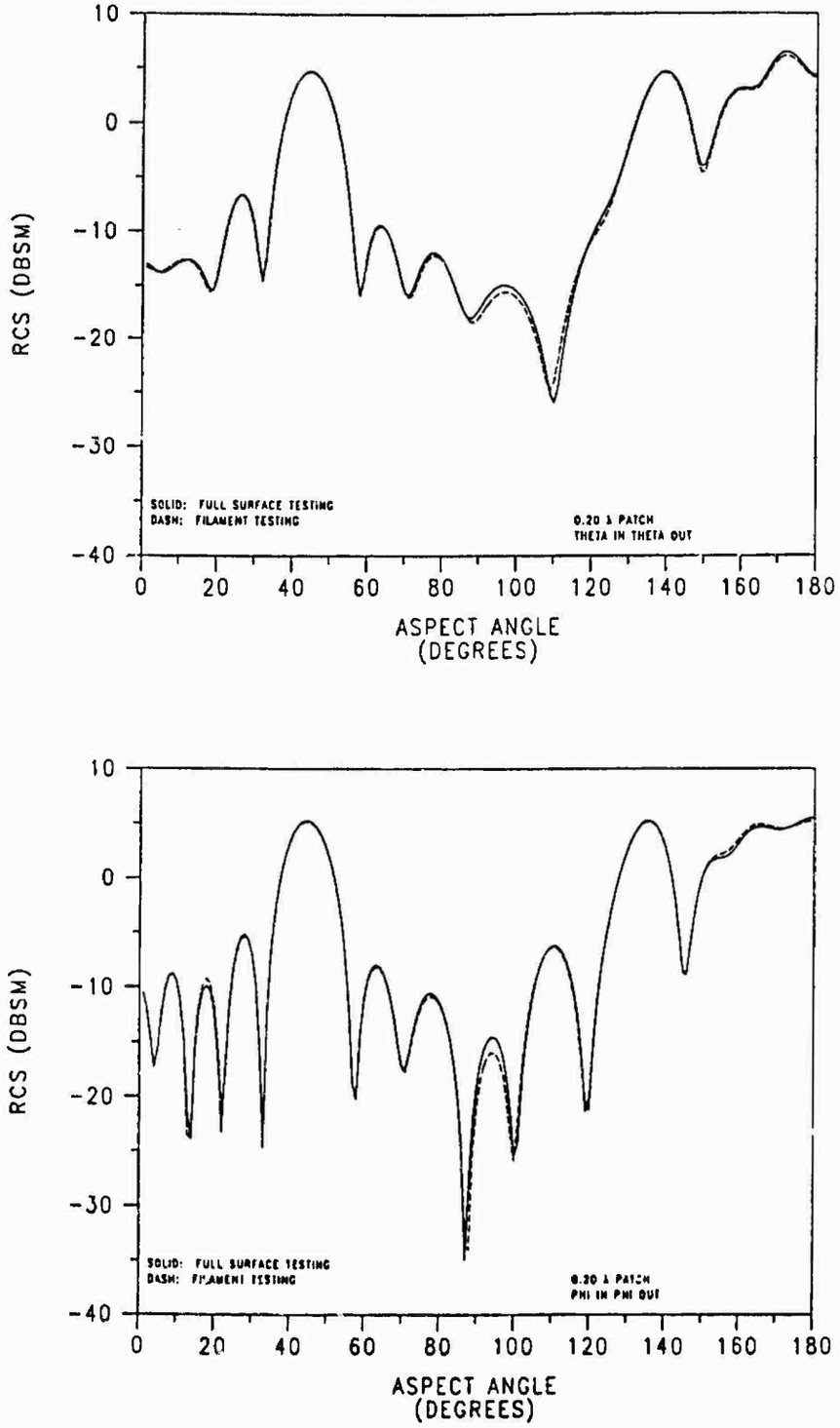

FIGURE 4-3. MONOSTATIC RCS OF 9" DIHEDRAL AT 3 GHZ
FILAMENT VERSUS FULL SURFACE TESTING COMPARISON

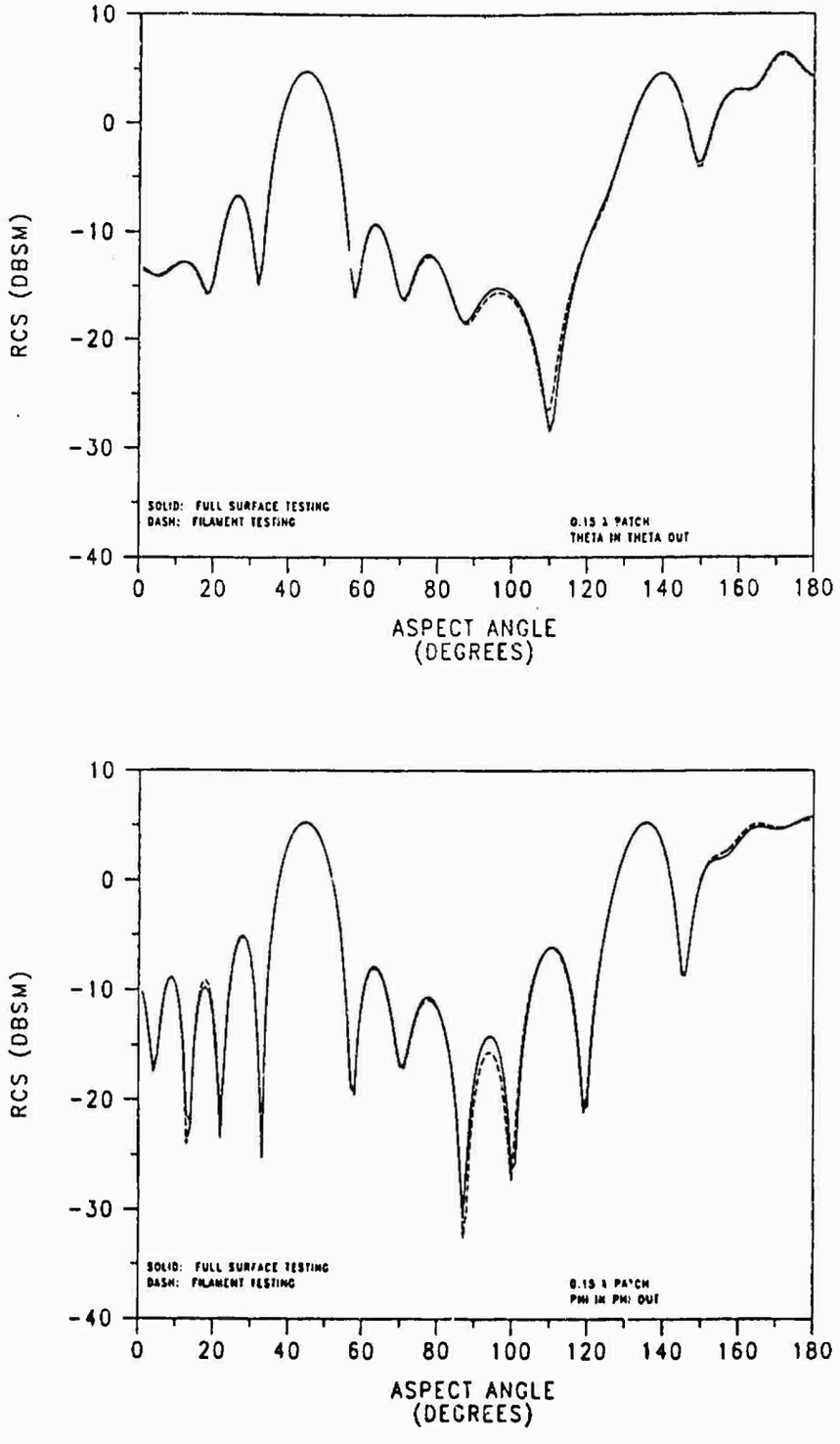

FIGURE 4-4. MONOSTATIC RCS OF 9" DIHEDRAL AT 3 GHZ
FILAMENT VERSUS FULL SURFACE TESTING COMPARISON

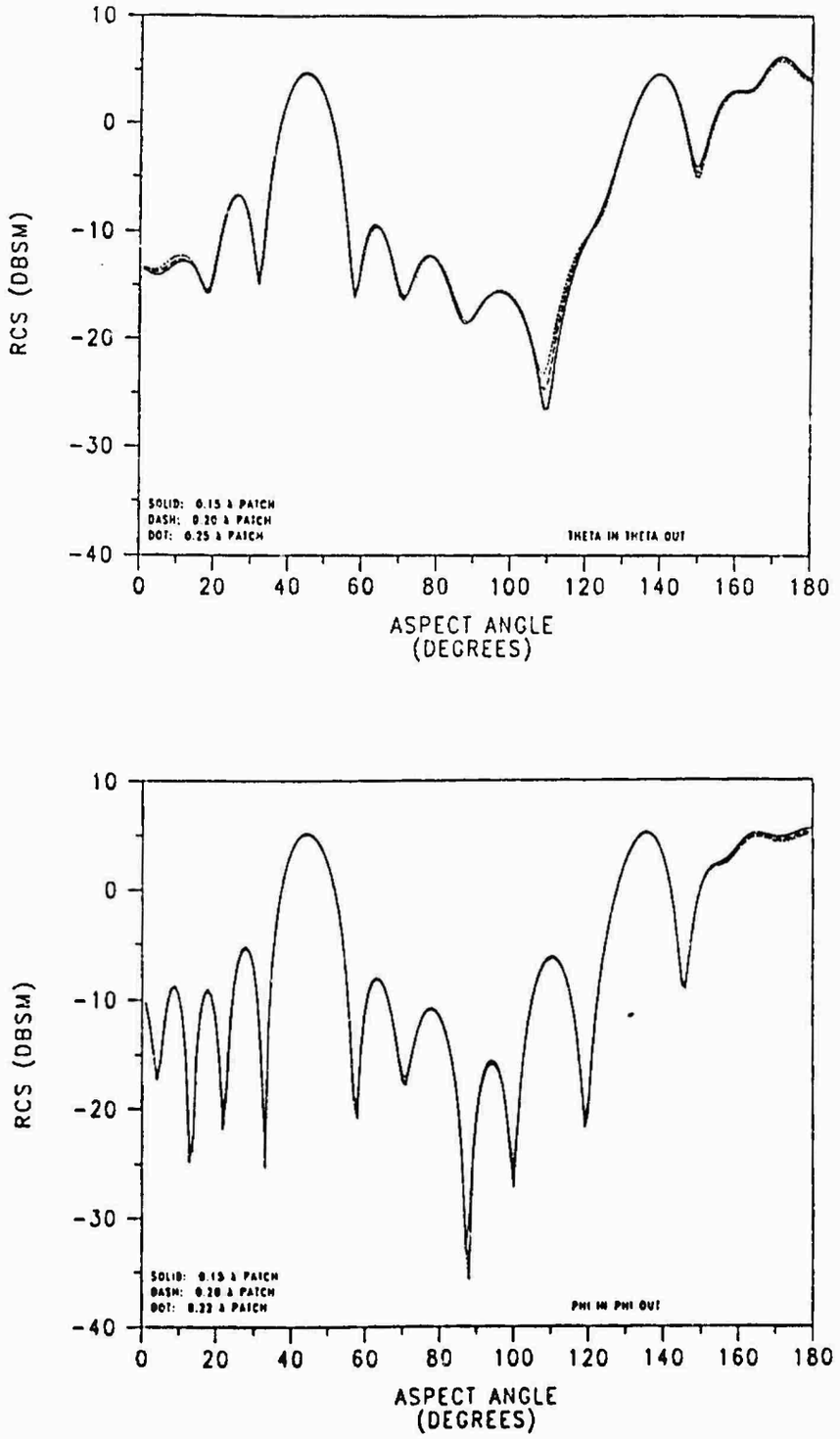

FIGURE 4-5. MONOSTATIC RCS OF 9" DIHEDRAL AT 3 GHZ
PATCH SIZE COMPARISON FOR FILAMENT TESTING

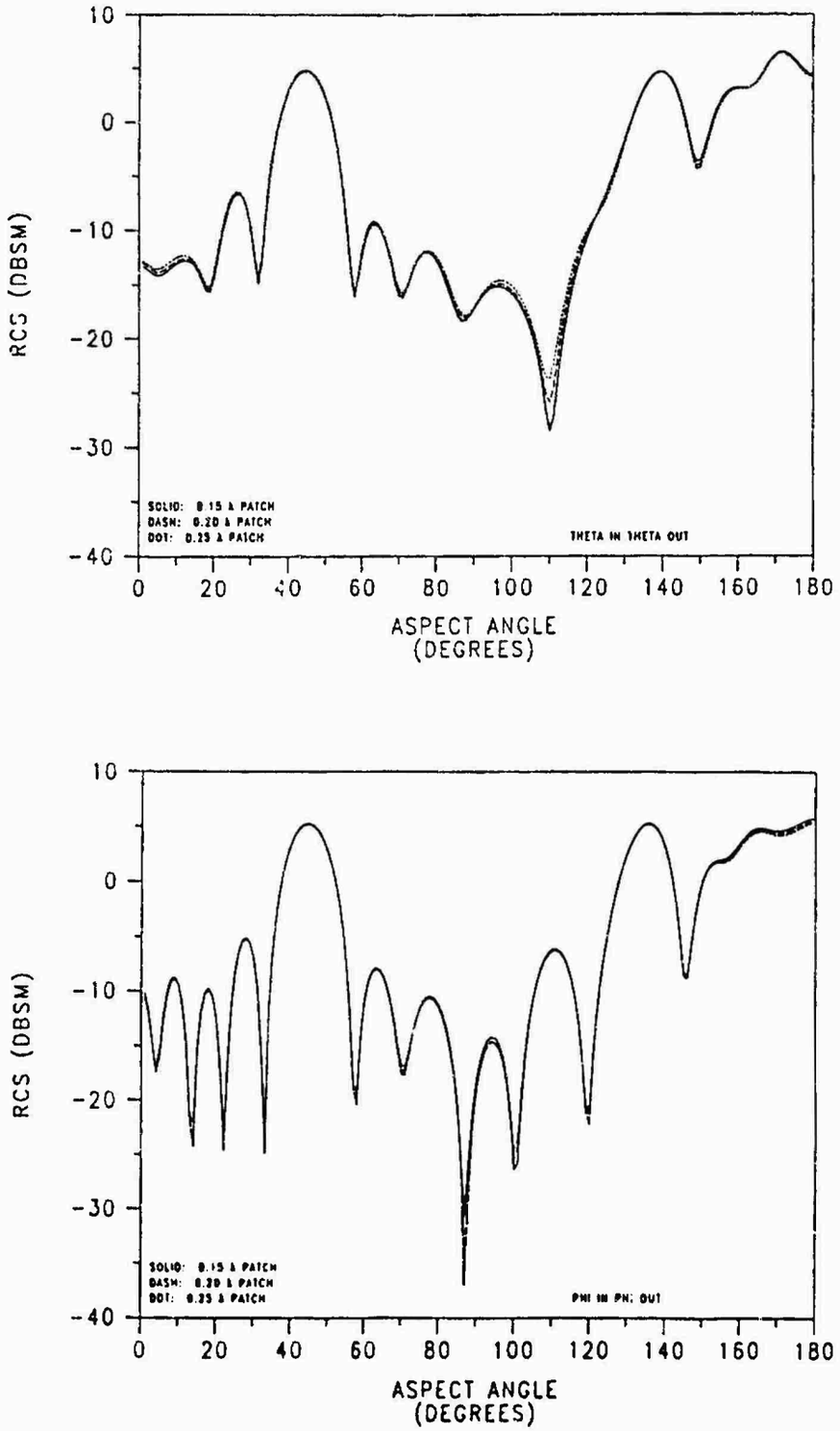

FIGURE 4-6. MONOSTATIC RCS OF 9" DIHEDRAL AT 3 GHZ
PATCH SIZE COMPARISON FOR FULL SURFACE TESTING

Noting that full surface testing yields the most accurate solution, a worst case comparison is made in Figure 4-7. Filament testing is used with a 0.25 wavelength patch, and full surface testing is used with a 0.15 wavelength patch. For theta in theta out, the greatest difference of approximately 5 dB is at 110°, and for phi in phi out, the greatest difference of about 5 dB is at 89°. There is good agreement elsewhere, especially considering the fact that this is a worst case comparison.

UTD Code Solutions

The UTD code used is a two dimensional model, and solves up to third order effects including at most double diffraction. All of the diffraction and reflection mechanisms up to the third order are included when either the expression 'DD Term Included' or 'UTD with All Terms' is used, and all except the double diffraction mechanism are included when 'DD Term Excluded' is specified. When the interior angle of the dihedral is 90°, the code does not include diffraction at the junction of the two plates, thus the only diffraction effects are from the two outer edges of the dihedral as shown in Figure 4-8.

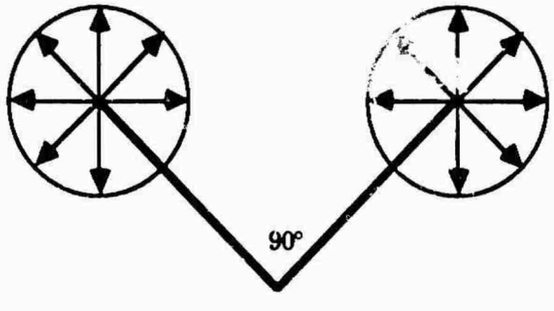

Figure 4-8 Diffraction Mechanisms

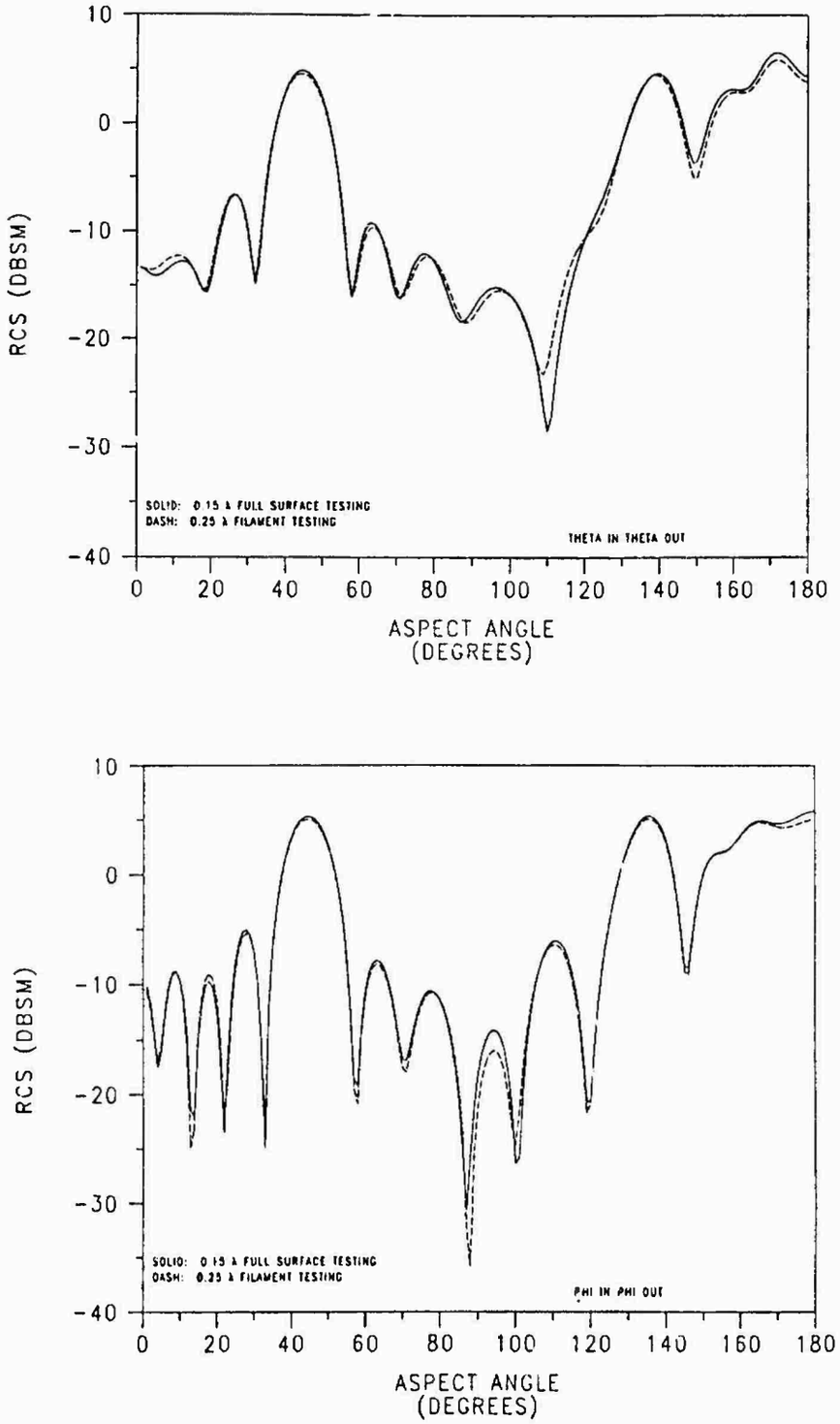

FIGURE 4-7. MONOSTATIC RCS OF 9" DIHEDRAL AT 3 GHZ
FILAMENT VERSUS FULL SURFACE TESTING COMPARISON

Figure 4-9 shows a double diffraction term comparison at 2 GHz for both theta in theta out and phi in phi out polarization for the monostatic case. At 135° and 180° for theta in theta out, the solution diverges to infinity when all the terms are included. The solution blows up at 135° because the observation point lies on the reflection shadow boundary (RB) of one of the plates as seen in Figure 4-10. Essentially, a flat plate is seen, and if the code could realize that fact, then the solution would converge. The problem is the code is still using the diffraction terms from the outer edges of the two plates.

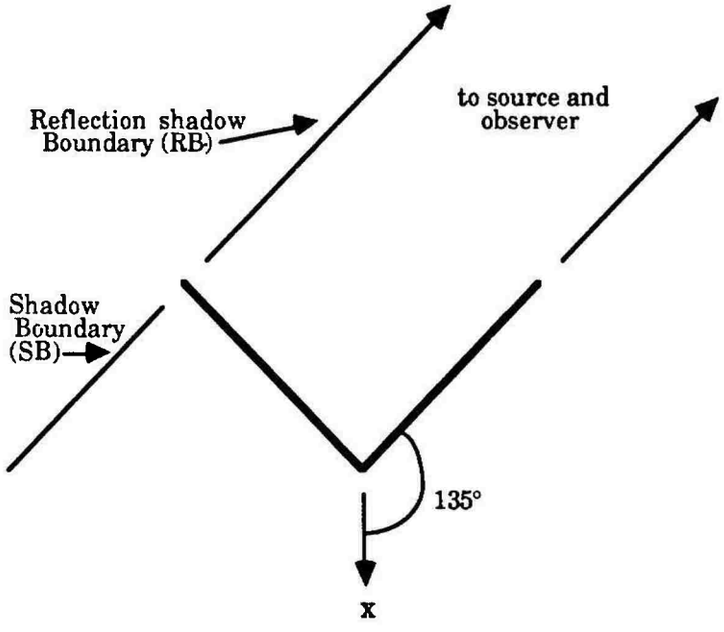

Figure 4-10 Dihedral Reflection Boundary

When the observation point approaches a reflection boundary (RB), the diffraction coefficients tend toward infinity. When a flat plate is seen, the diffraction at the two edges have opposite signs, thus the infinities cancel and the solution converges. But the code sees one edge at the RB

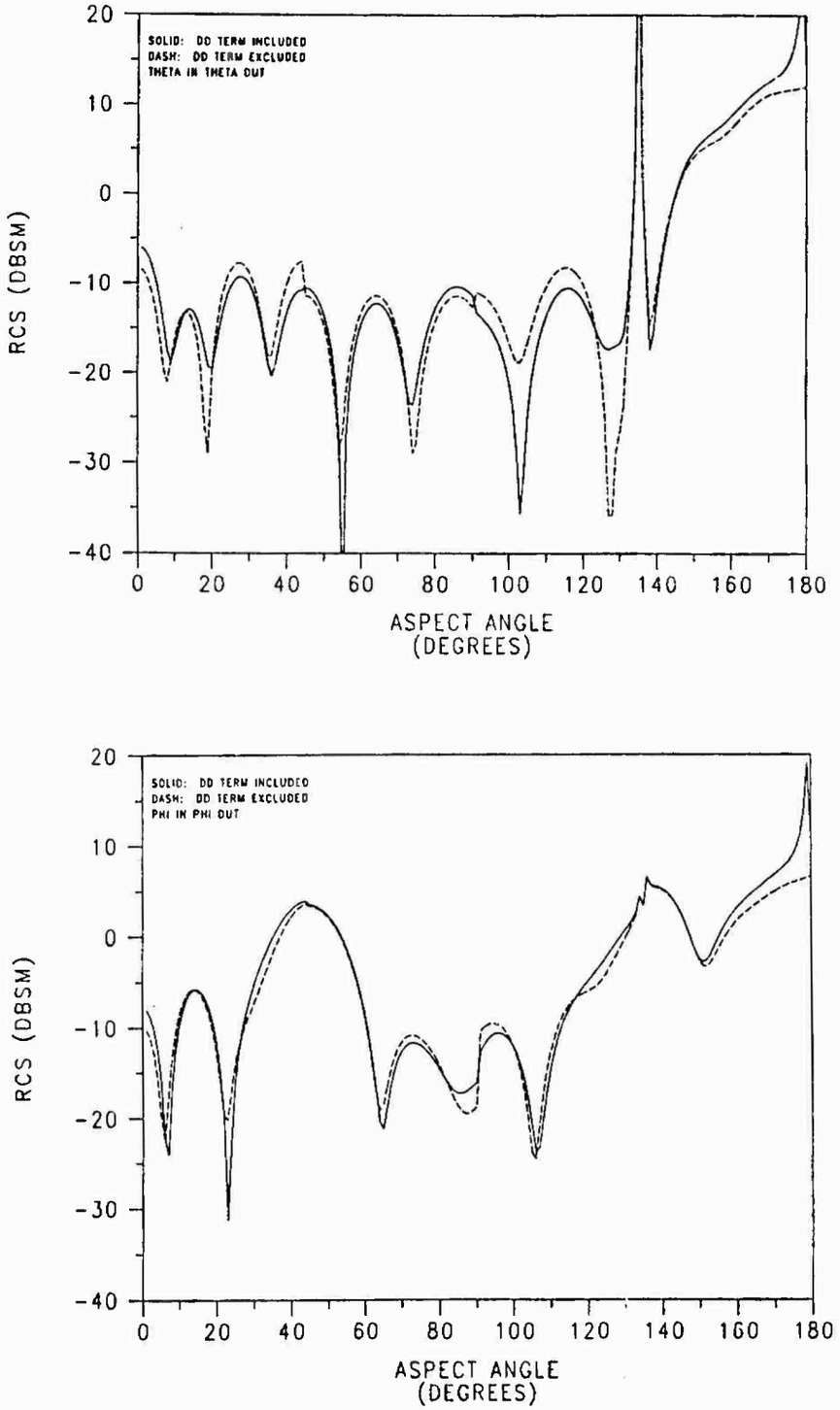

FIGURE 4-9. MONOSTATIC RCS OF 9" DIHEDRAL AT 2 GHZ
UTD DOUBLE DIFFRACTION TERM COMPARISON

and the edge of the second plate is seen edge on, thus giving one infinite and one finite coefficient. To overcome this problem, the code should treat the diffraction at the junction of the plates as a second edge of the plate with the infinite diffraction coeff nt. This would insure convergence of the solution.

At 180° the solution diverges for a similar reason. The problem at 180° is with the double diffraction term. The second edge lies on the RB of the first edge, and the observation point lies on the RB of the second edge as seen in Figure 4-11.

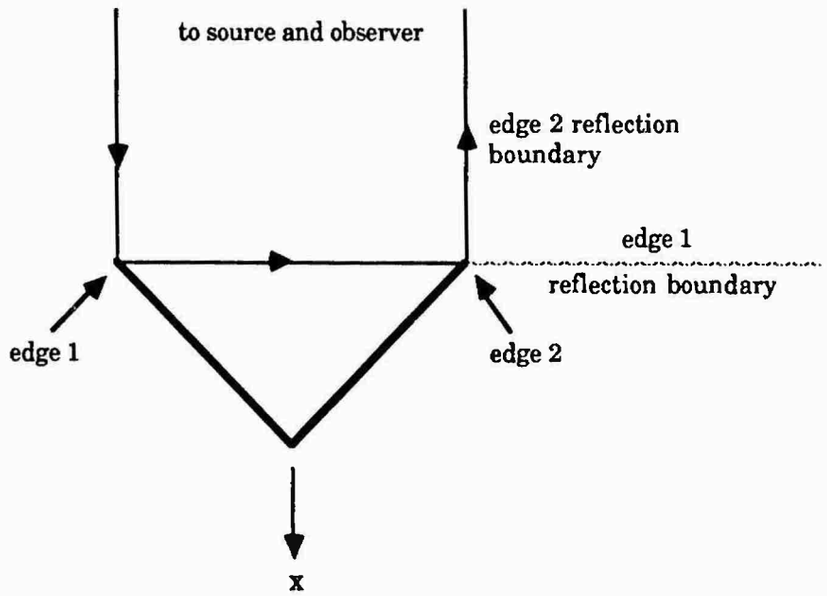

Figure 4-11 Dihedral DD Reflection Boundary

This problem is not as easy to alleviate as the reflection boundary problem at 135°. A uniform double diffraction coefficient that is well behaved across the reflection boundary is needed. Without the DD term the solution converges at 180° as seen in Figure 4-9. However, excluding the

DD term is not without consequence. Accuracy is lost throughout the pattern, and not just in the region near 180°.

Figure 4-12 shows the monostatic DD term comparison at 3 GHz, where the effect of the DD term is more apparent. By excluding the DD term, the divergence of the solution near 180° is alleviated, but the degradation of the pattern elsewhere has increased greatly. The fact that the pattern changes when the DD term is excluded signifies the importance of the double diffraction mechanism in the RCS of the dihedral corner reflector. The regions where the DD mechanism is more prominent are shown by larger differences between the DD term included and excluded patterns.

Figure 4-13 shows another monostatic DD term comparison at 10 GHz. From 3 GHz to 10 GHz the wavelength shortens; thus, the distance for a 360° phase shift also shortens, which causes the RCS pattern to exhibit more oscillations. The increased oscillation makes the task of pattern comparisons a little more difficult. However, the degradation of the RCS pattern from excluding the DD term is still obvious, especially for theta polarization. All of the monostatic patterns, regardless of frequency, have the same problem of the reflection shadow boundary at 135° and 180° causing the solution to diverge.

What happens when the geometry is changed to a bistatic case? The observation point leads the source point by a specified angle when the bistatic case is stated. Figure 4-14 shows the 90° bistatic RCS of the dihedral at 3 GHz for theta in theta out and phi in phi out polarization. With the DD term included the theta in theta out pattern is well behaved, except for finite discontinuities at 180° and 225°. Excluding the DD term

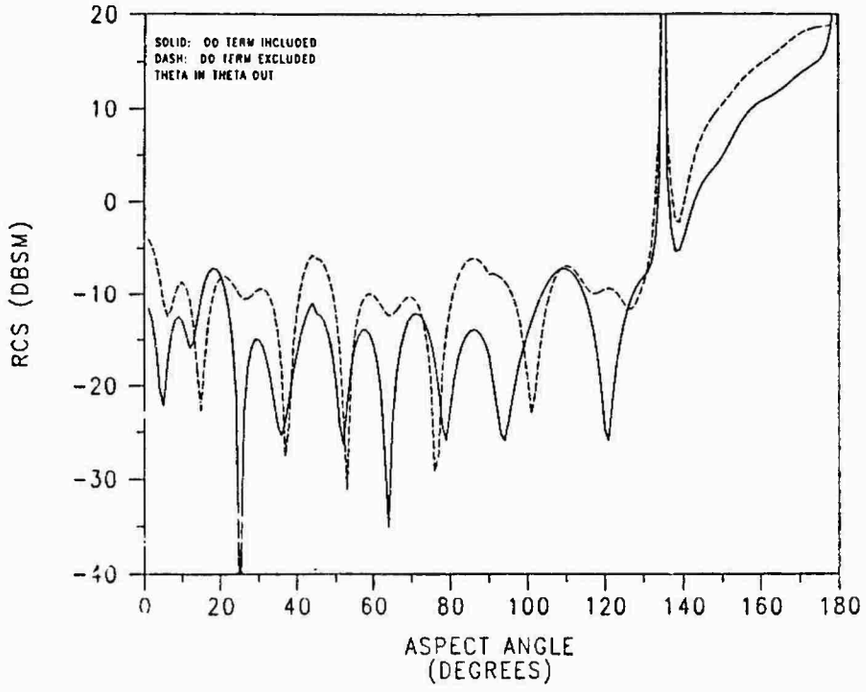

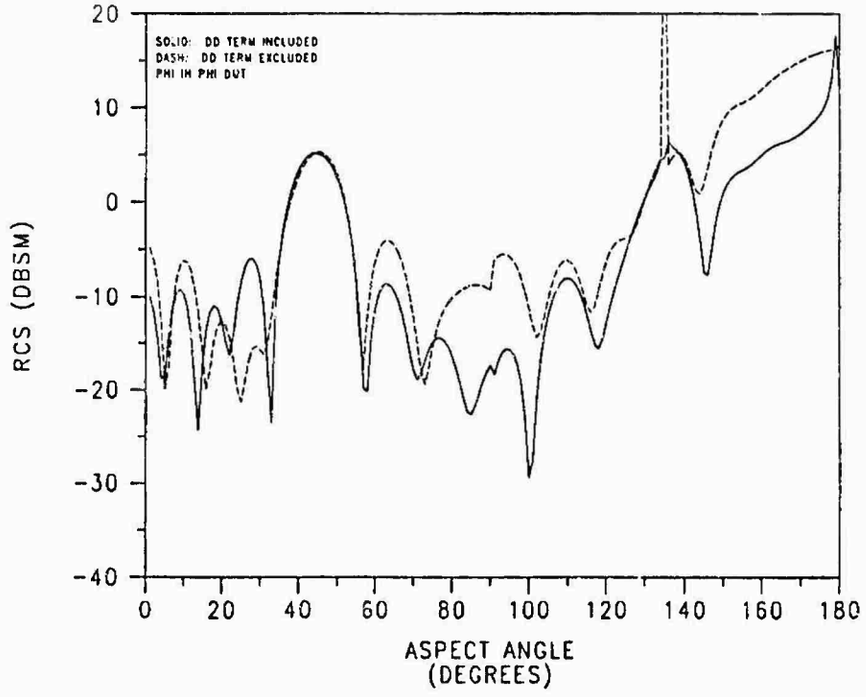

FIGURE 4-12. MONOSTATIC RCS OF 9" DIHEDRAL AT 3 GHZ
UTD DOUBLE DIFFRACTION TERM COMPARISON

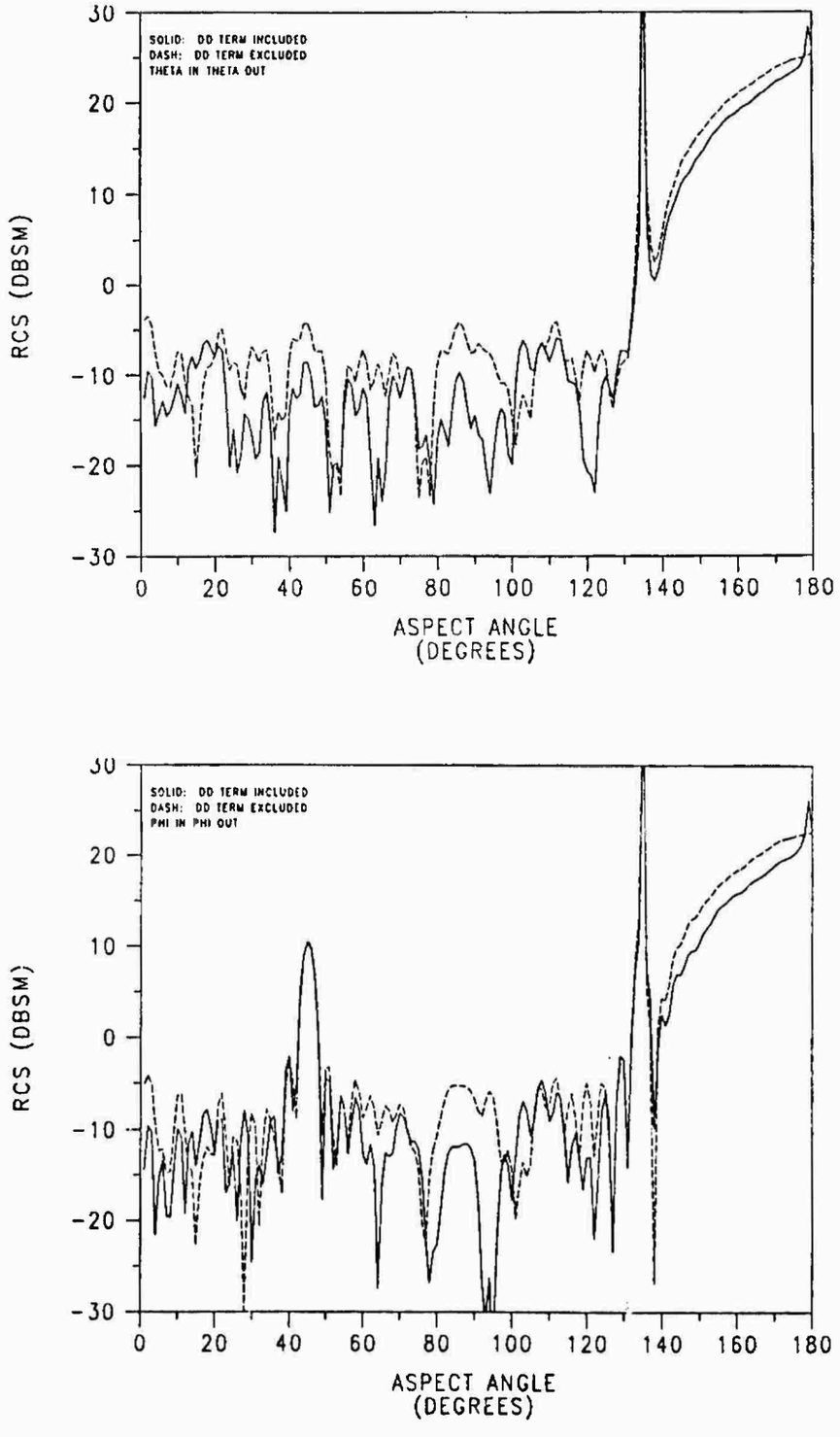

FIGURE 4-13. MONOSTATIC RCS OF 9" DIHEDRAL AT 10 GHZ
UTD DOUBLE DIFFRACTION TERM COMPARISON

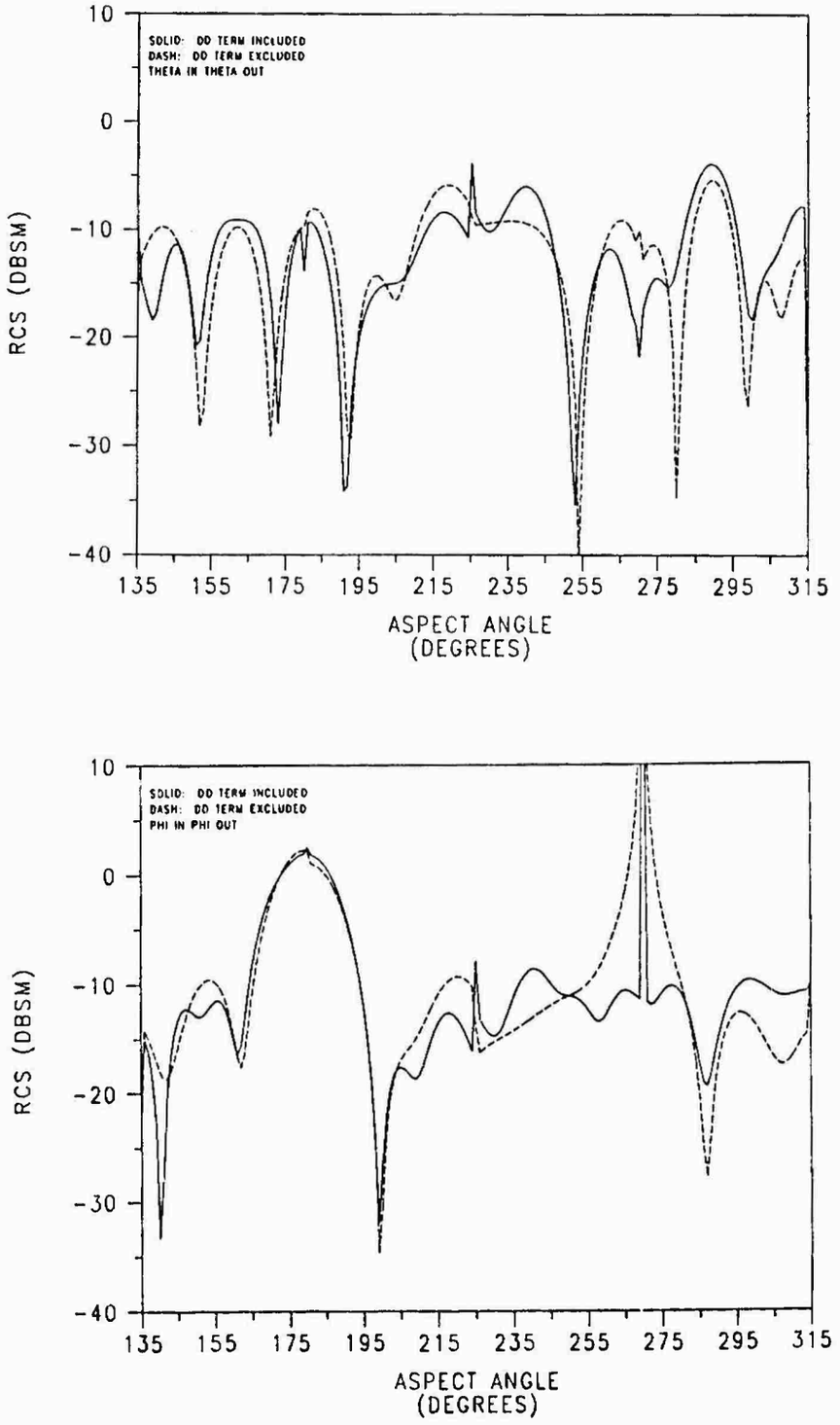

FIGURE 4-14. 90 DEGREE BISTATIC RCS OF 9" DIHEDRAL AT 3 GHZ
UTD DOUBLE DIFFRACTION TERM COMPARISON

removes the abrupt shifts in the pattern, but degrades the remainder of the pattern. With the DD term included the phi in phi out also exhibits finite discontinuities at 180° and 225°, but an infinite discontinuity exists at 270°. Here the source is at 180° which is looking down the center of the dihedral and the observation point is directly to the side. The problem arises from the fact that edge 1 is on the reflection shadow boundary of edge 2, and the observation point is also on the RB as well as on the shadow boundary of edge 1, as seen in Figure 4-15. Excluding the DD term does not alleviate the problem, and even worsens the divergence of the solution in the region near 270°.

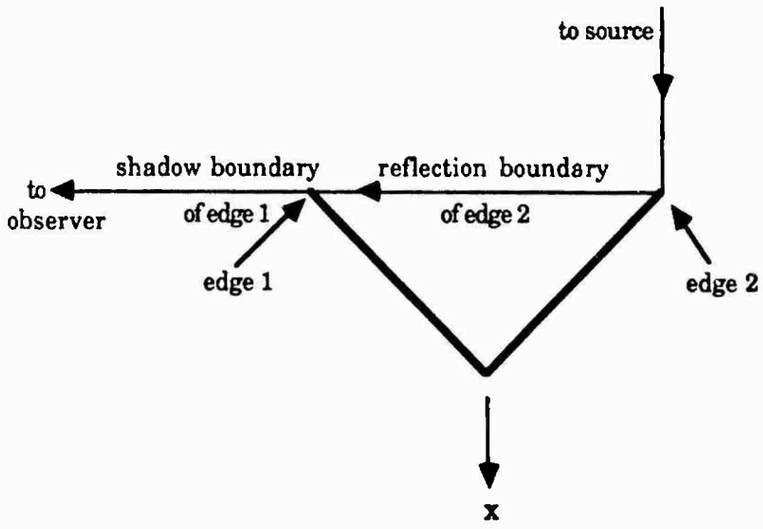

Figure 4-15 Bistatic Reflection Boundary

Figure 4-16 shows the 90° bistatic DD term comparison at 10 GHz for theta in theta out and phi in phi out polarization. Again, the finite discontinuity is present at 225° for both polarizations, and the phi polarization has the infinite discontinuity at 270°. The importance of the

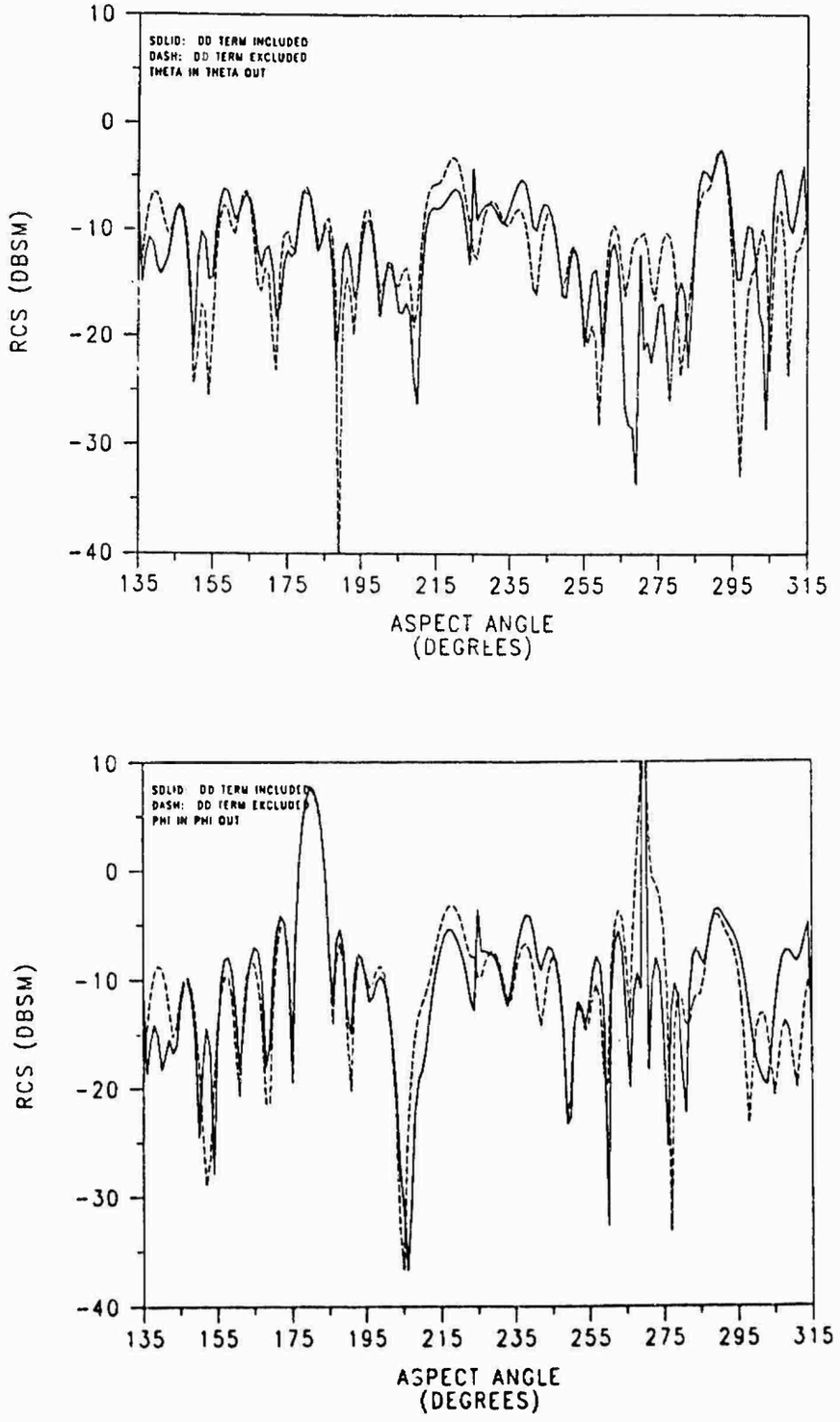

FIGURE 4-16. 90 DEGREE BISTATIC RCS OF 9" DIHEDRAL AT 10 GHZ
UTD DOUBLE DIFFRACTION TERM COMPARISON

double diffraction mechanism for the bistatic case can be seen by the differences between the RCS patterns when the DD term is included and excluded at both 3 GHz and 10 GHz.

No improvement is gained by excluding the DD term for the bistatic case, so can the discontinuities be taken care of another way? Possibly the observer could be taken off the shadow and reflection boundaries by changing the bistatic angle to an angle slightly off 90°. Figure 4-17 shows a comparison between a 90° and 89.7° bistatic angle for theta in theta out and phi in phi out polarization. For theta polarization, the glitch at 180° was completely removed, and the glitch at 225° was greatly reduced, all without altering the overall pattern. For phi polarization, the glitch at 180° was worsened, the glitch at 225° was reduced, and the discontinuity at 270° was worsened and made to appear like the 90° bistatic without the DD term.

Shifting the bistatic angle a little more, Figure 4-18 shows a comparison between 90° and 89.5° for 3 GHz. For theta polarization, the glitch at 180° was removed, the glitch at 225° was reduced, but now a new glitch was introduced at 270°. For phi polarization, the glitch was removed at 180°, reduced at 225°, and the discontinuity was again worsened at 270°. Patterns were also made for bistatic angles of 89.3° and 89.0°, but they proved to be too far off of 90° to give accurate results, and are not included in this thesis. The 89.7° bistatic yielded best results for theta polarization, and the 90° bistatic yielded the best results for phi polarization at 3 GHz.

Figure 4-19 shows a comparison between 90° and 89.7° at 10 GHz. For theta polarization, the pattern changed most at 225° and 270° when the bistatic angle was shifted to 89.7°. At 225° it is difficult to tell if there was pattern improvement, at 90° the glitch was in the positive direction and

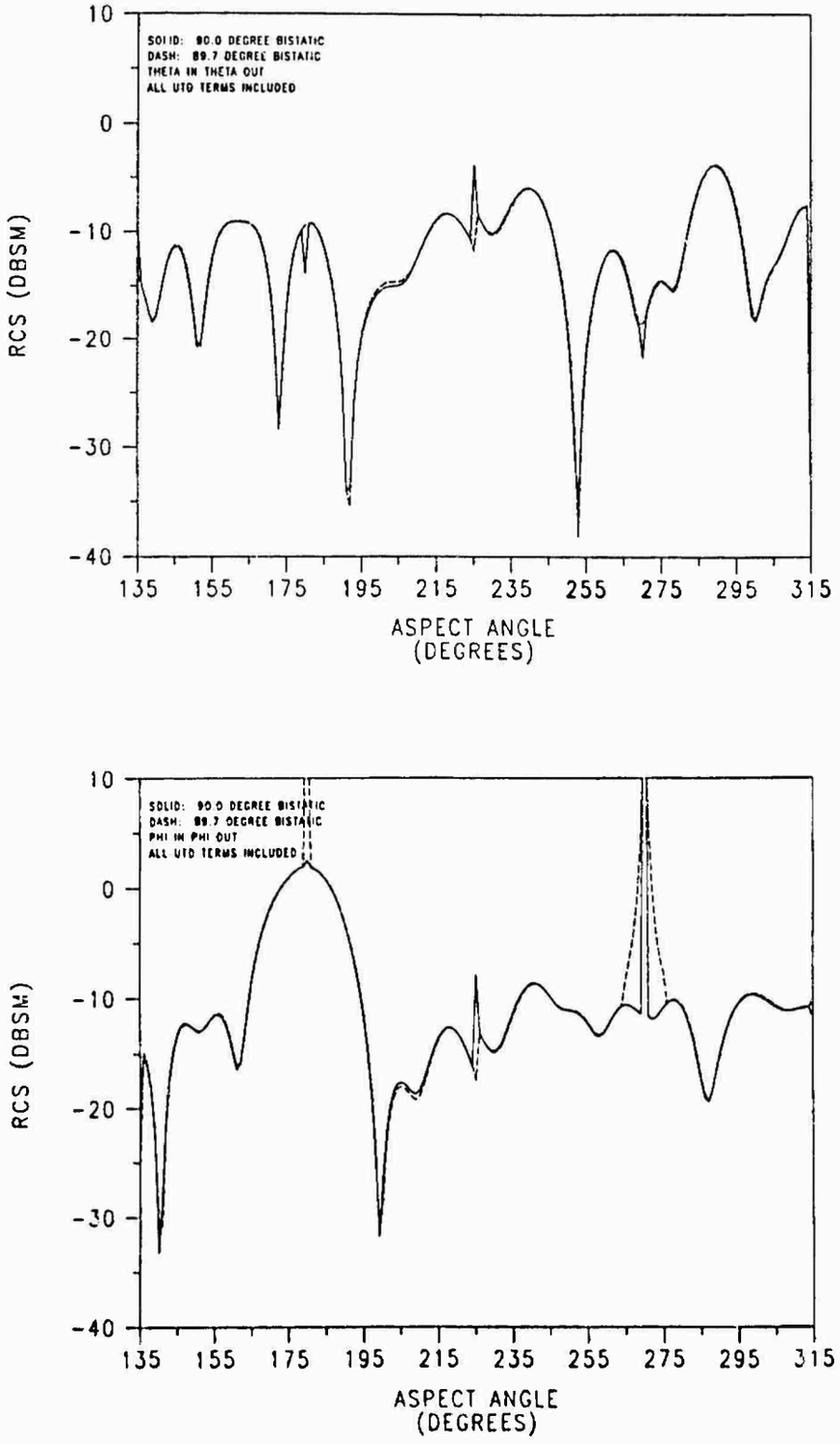

FIGURE 4-17. BISTATIC RCS OF 9" DIHEDRAL AT 3 GHZ
90.0 AND 89.7 BISTATIC ANGLE COMPARISON

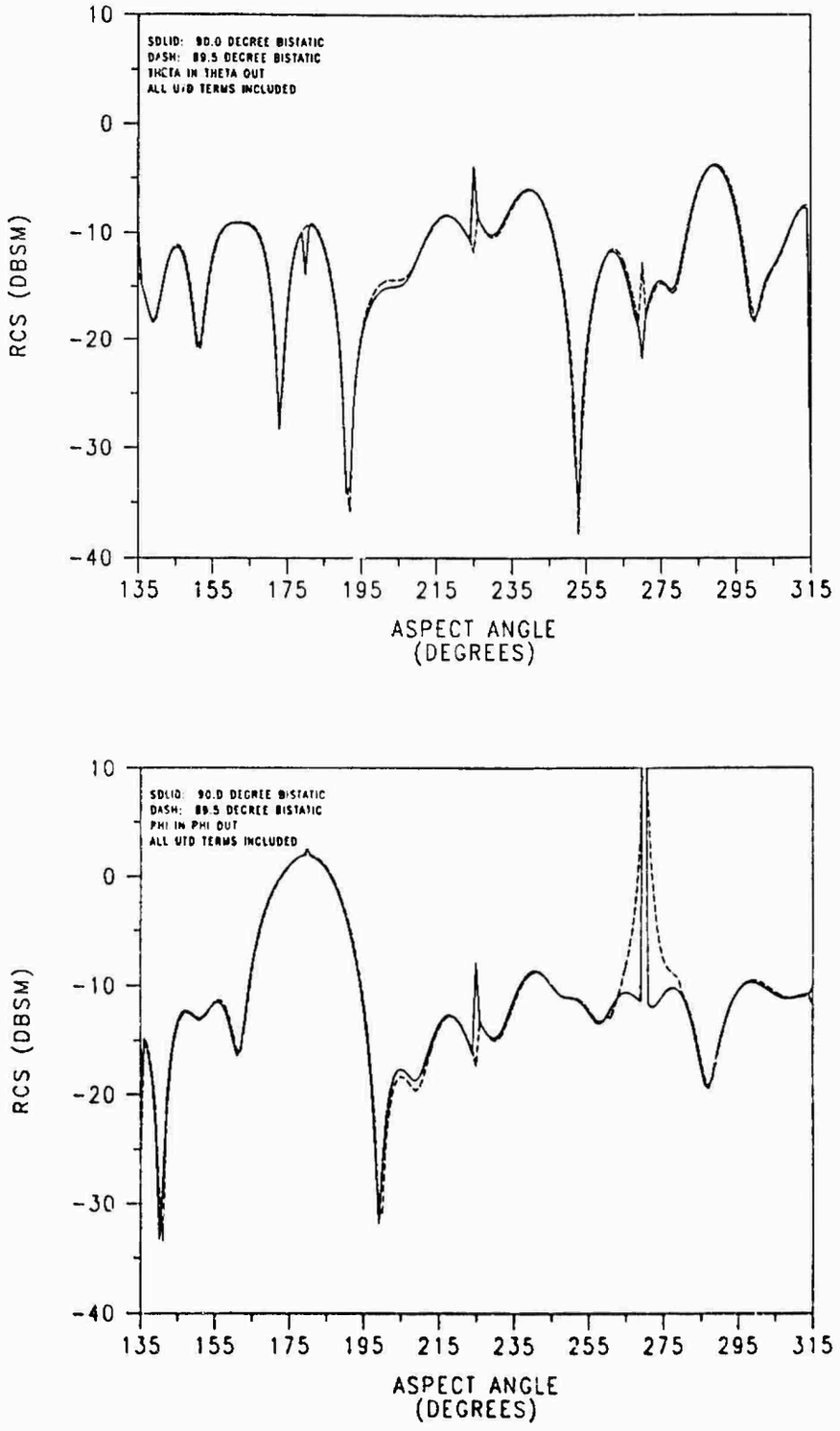

FIGURE 4-18. BISTATIC RCS OF 9" DIHEDRAL AT 3 GHZ
90.0 AND 89.5 BISTATIC ANGLE COMPARISON

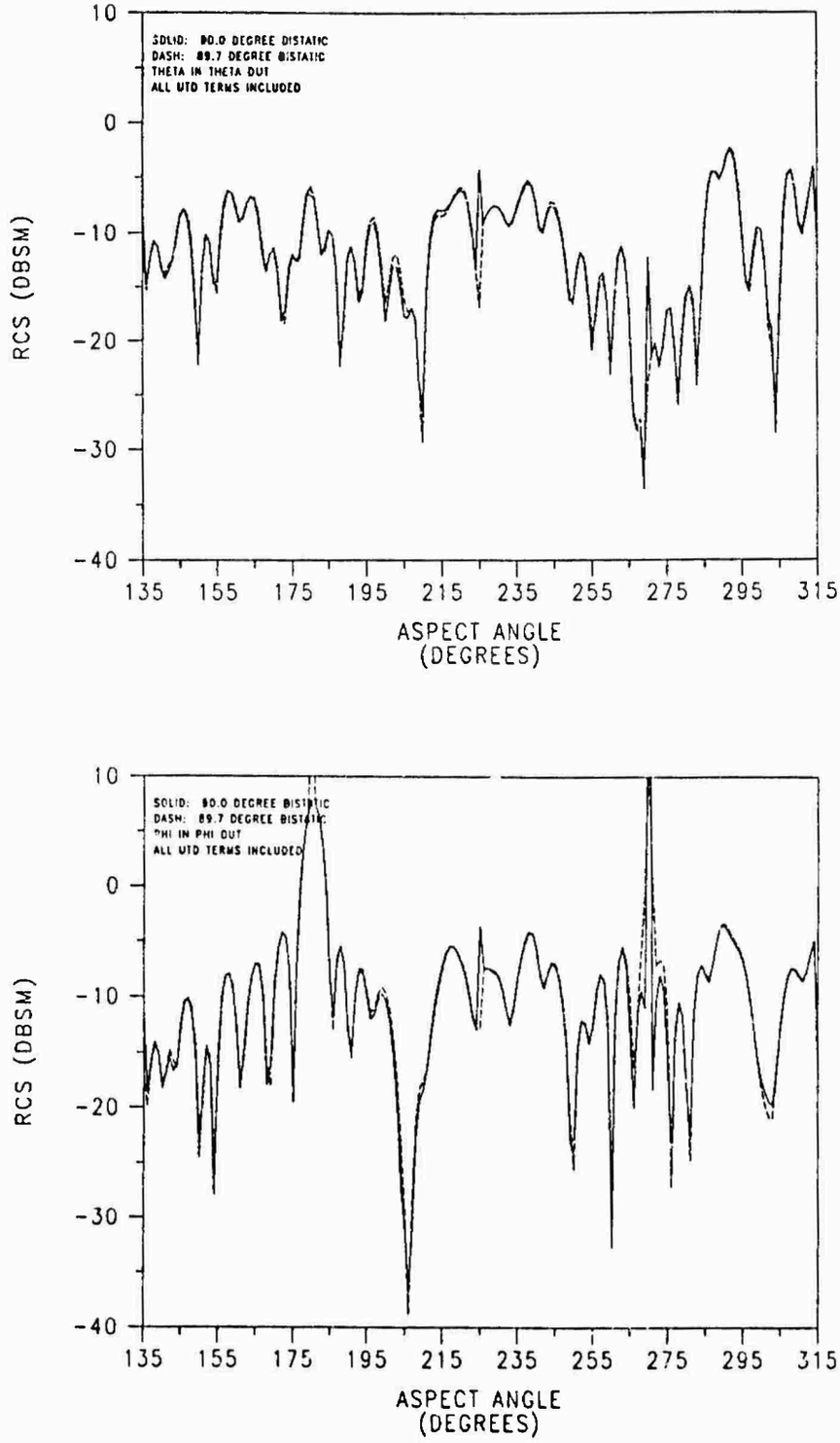

FIGURE 4-19. BISTATIC RCS OF 9" DIHEDRAL AT 10 GHZ
90.0 AND 89.7 BISTATIC ANGLE COMPARISON

when the bistatic angle changed to 89.7° the glitch reversed to the negative direction. Since the pattern was going negative before 225° and going positive after 225° leads one to feel more confident in the 89.7° pattern since the glitch also exhibits the same characteristics before and after 225°. For phi polarization, the 10 GHz patterns responded the same as the 3 GHz patterns when the bistatic angle was changed to 89.7°. The pattern blew up at 180° and the glitch was removed at 225° when the bistatic angle was shifted to 89.7°. At 270° the discontinuity was not reduced by the new bistatic angle, instead the discontinuity was widened and appeared like the pattern with the DD term excluded.

Changing the bistatic angle to 89.5°, Figure 4-20 shows the comparison with 90° for both theta and phi polarization. For theta polarization, the pattern exhibited the same change at 225° as the 89.7° comparison, but elsewhere the pattern differed. The discontinuity at 270° was unchanged, and minor changes appeared throughout the pattern. The extra pattern changes that were not experienced by the 89.7° pattern and the patterns at 3 GHz were again due to the fact that the distance for a 360° phase shift is shorter at 10 GHz, thus more sensitive to changes in the angles, both aspect and bistatic . For phi polarization, the pattern was well behaved at 180°, the glitch was removed at 225°, and the discontinuity was widened at 270°. The phi pattern also experienced the extra pattern changes due to the angle sensitivity. The best patterns for the bistatic case at 10 GHz were the 89.7° for theta polarization, and 90° for phi polarization.

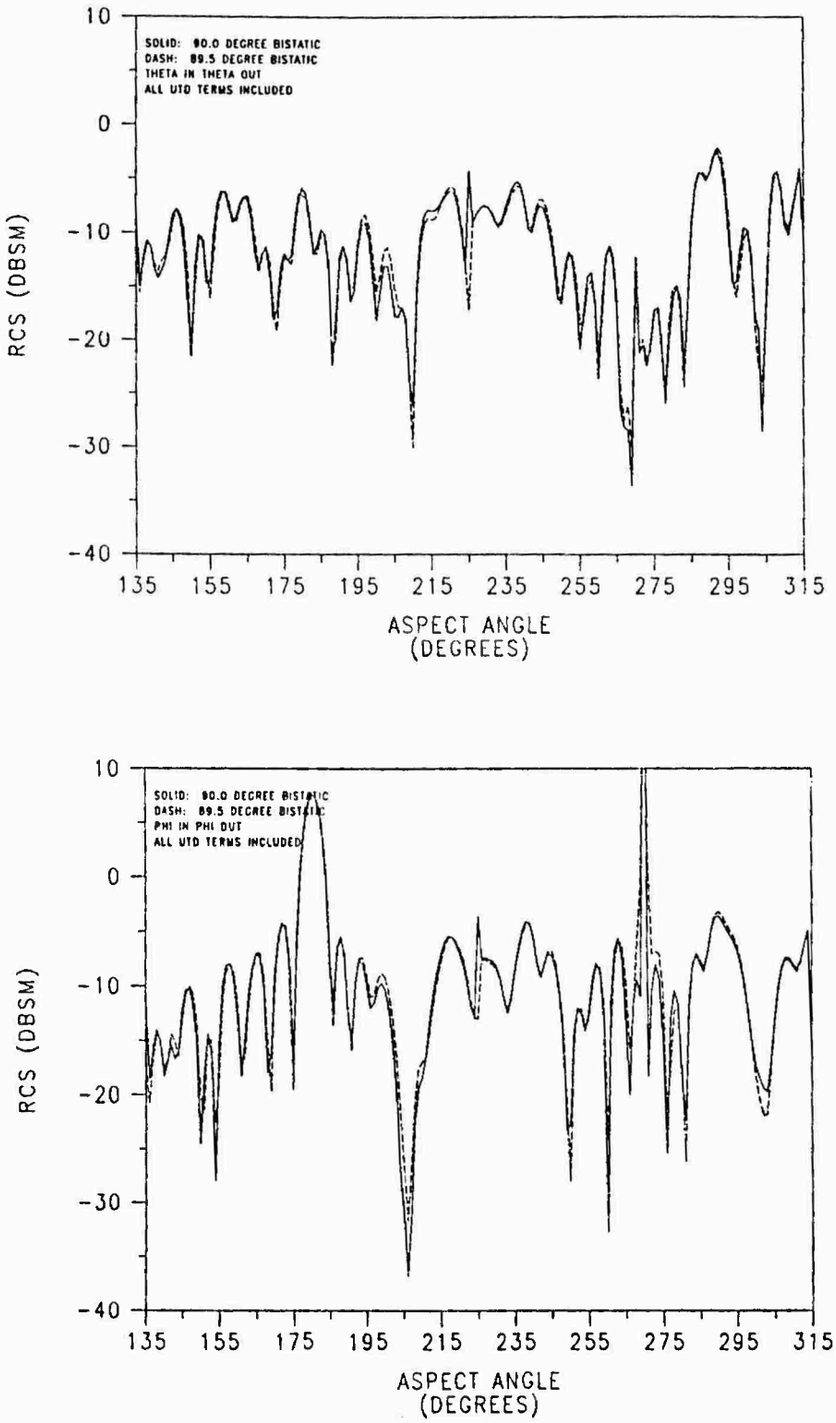

FIGURE 4-20. BISTATIC RCS OF 9" DIHEDRAL AT 10 GHZ
90.0 AND 89.5 BISTATIC ANGLE COMPARISON

MOM - UTD Comparison

Now that the MOM and UTD codes have been compared with themselves, how do they compare with each other? The MOM is more accurate than UTD, but the increased accuracy of MOM has the disadvantage of increased computer time. The UTD code is two dimensional so it cannot provide cross polarization information, while the MOM provides all polarization components. At 2 GHz, MOM with a 0.10 wavelength full surface patch test took approximately 4 hours of CPU time on the VAX 11/785 with 14 megabytes of main memory, whereas the UTD only took 6 seconds of CPU time. One run with the MOM code provided patterns for all polarization combinations, where the UTD code only provided one copolarization combination.

Figure 4-21 shows the comparison between MOM and UTD for the monostatic RCS at 2 GHz for theta and phi polarization. The phi patterns compared very well, but what happened to the theta polarization? The problem was that the UTD code only calculated the diffraction from the outer edges of the dihedral, and did not include diffraction terms from the top and bottom edges since there are no top and bottom edges in a two dimensional model. With the MOM UTD comparison, the task of finding the regions where these missing terms were most needed was simplified. For theta polarization, the region where the extra terms were needed included almost the entire pattern. This was reasonable since the energy diffracted when the electric field is parallel to the edge is less than when the electric field is perpendicular, corresponding to theta and phi polarization. This was exemplified by Figure 4-21, where the UTD theta

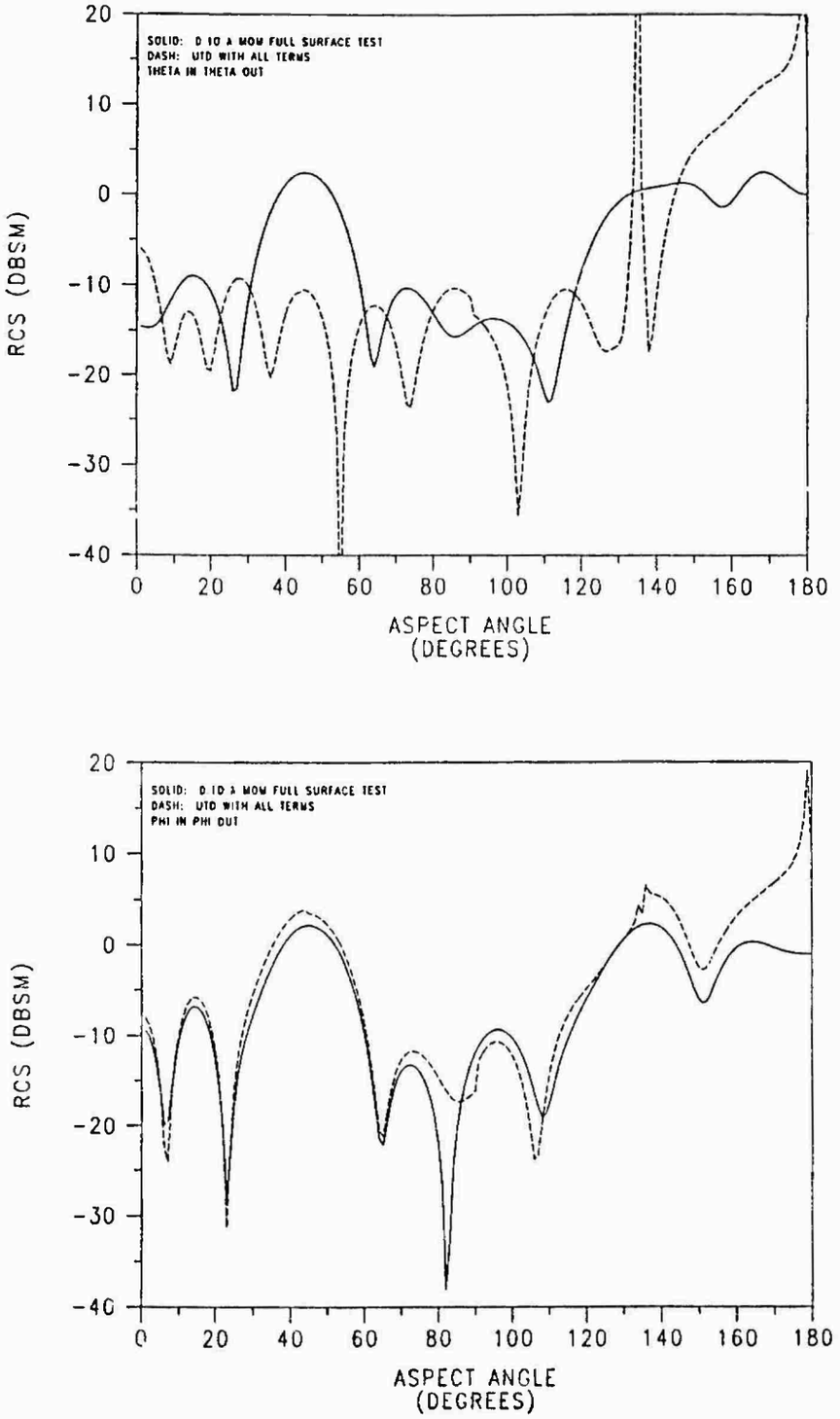

FIGURE 4-21. MONOSTATIC RCS OF 9" DIHEDRAL AT 2 GHZ
MOM VERSUS UTD COMPARISON

polarization pattern is not as accurate, and the UTD phi polarization pattern is accurate when compared to the MOM solutions.

Figure 4-22 shows the comparison between MOM and UTD for the monostatic case at 3 GHz. Again, the UTD pattern compares well with the MOM solution for phi polarization and not so well for theta polarization. Figure 4-23 shows another comparison for the monostatic case at 10 GHz. The UTD departed from the MOM solution more for the theta polarization than the phi polarization, but the phi polarization was not as accurate as it was for 2 GHz and 3 GHz. Normally the UTD solution should improve in accuracy as the frequency is increased since UTD is a high frequency approximation. However, the missing diffractions terms had a greater effect on the pattern at 10 GHz than 2 GHz and 3 GHz.

Figure 4-24 shows the UTD MOM comparison for the bistatic case at 3 GHz. The UTD did not compare well to MOM for theta polarization, and did not compare as well for phi polarization as the monostatic case. The poor comparison indicated that more diffraction mechanisms were needed to accurately predict the RCS at bistatic angles.

Figure 4-25 shows the UTD MOM comparison for the bistatic case at 10 GHz. Once again there was poor correlation between the patterns for theta polarization, and fair correlation for phi polarization. The two dimensional UTD proved to be too much of a simplification for a three dimensional object like the dihedral corner reflector.

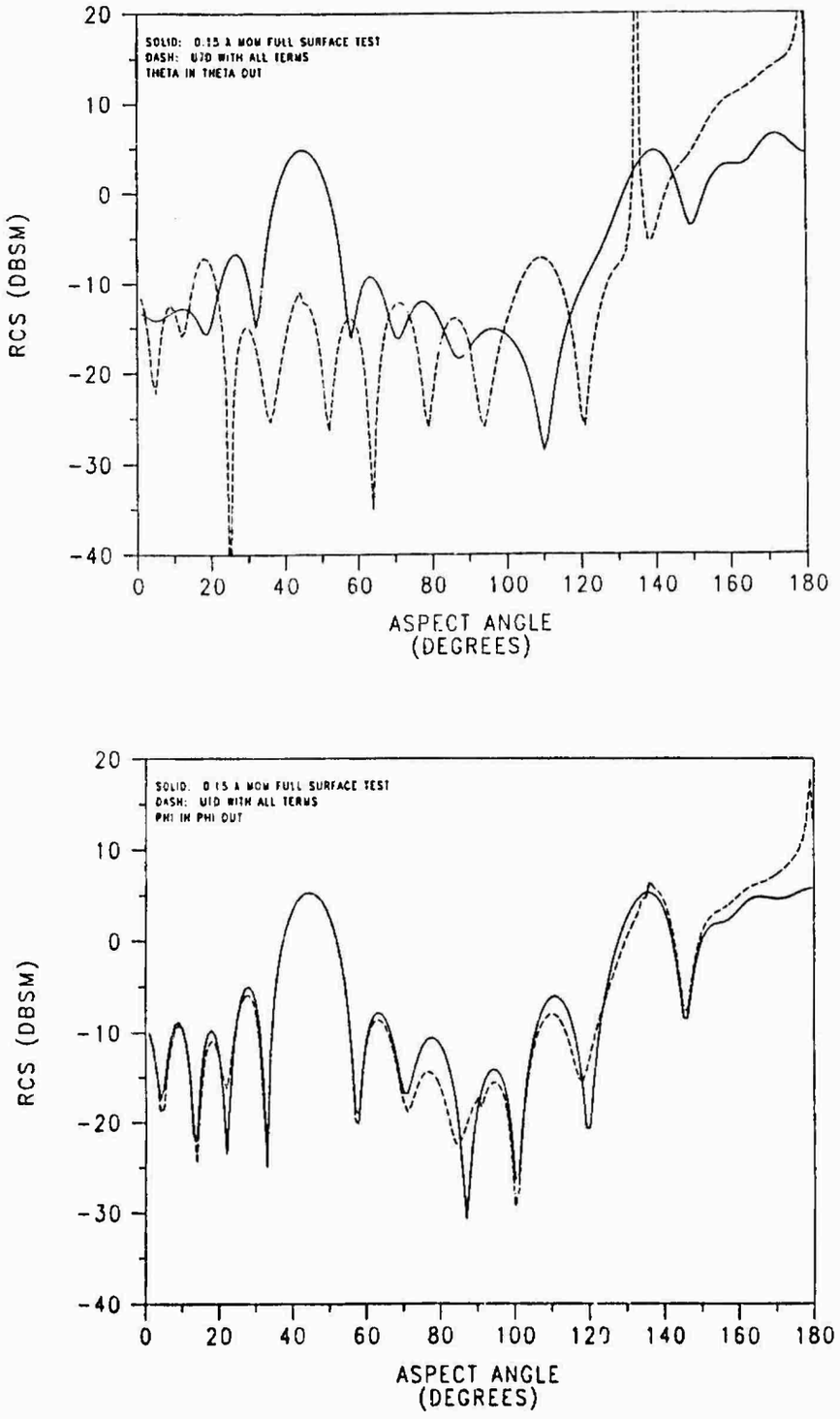

FIGURE 4-22. MONOSTATIC RCS OF 9" DIHEDRAL AT 3 GHZ
MOM VERSUS UTD COMPARISON

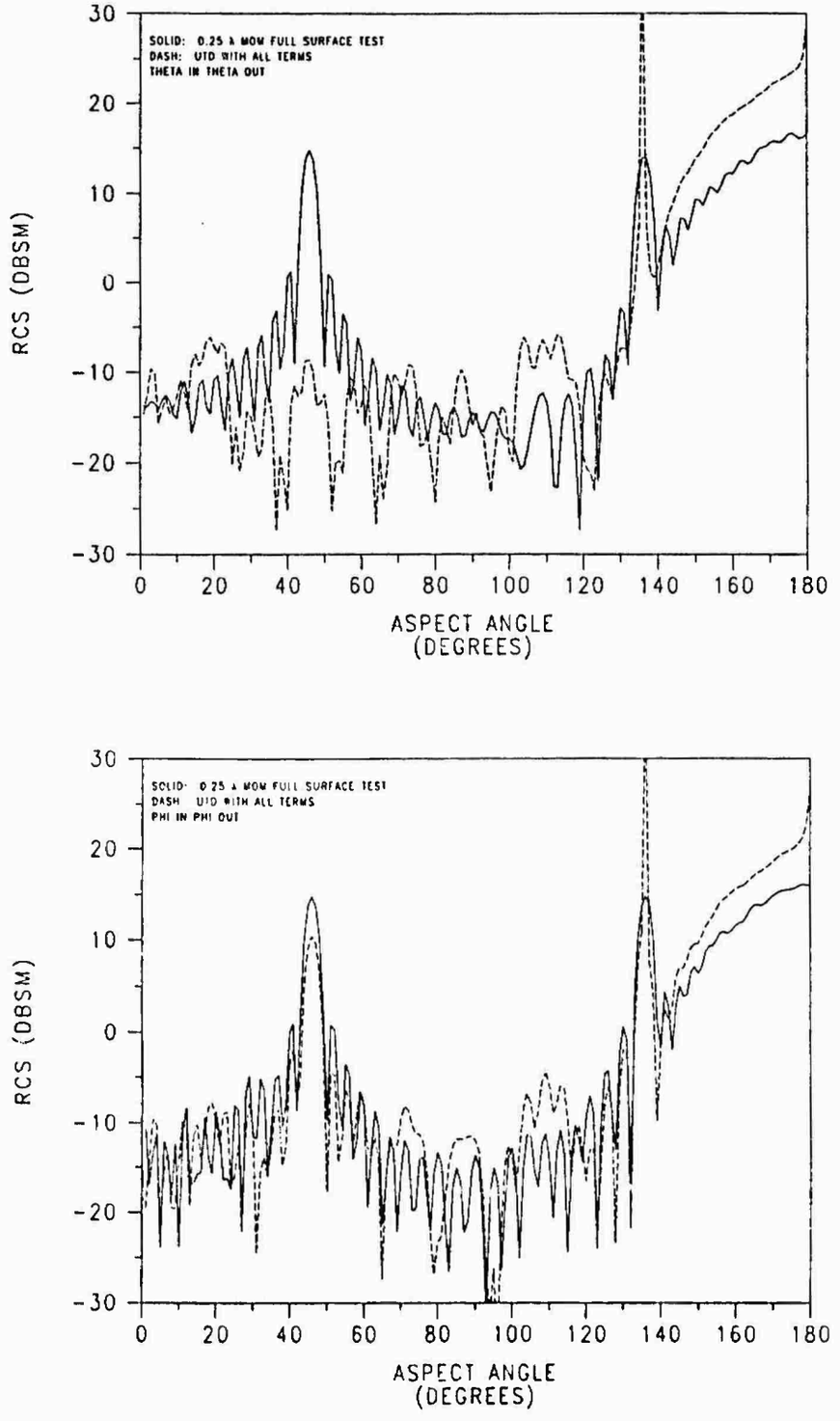

FIGURE 4-23. MONOSTATIC RCS OF 9" DIHEDRAL AT 10 GHZ MOM VERSUS UTD COMPARISON

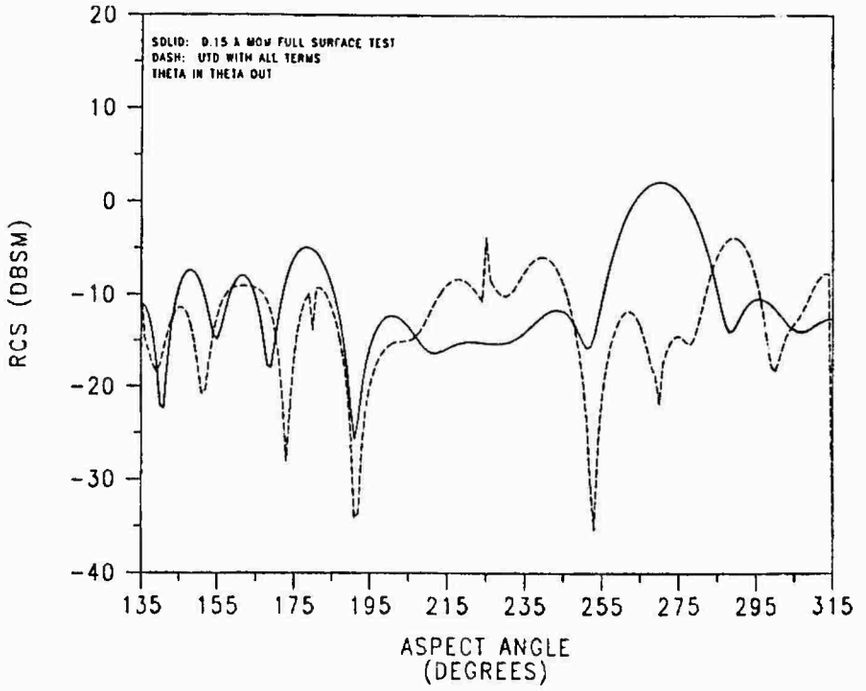

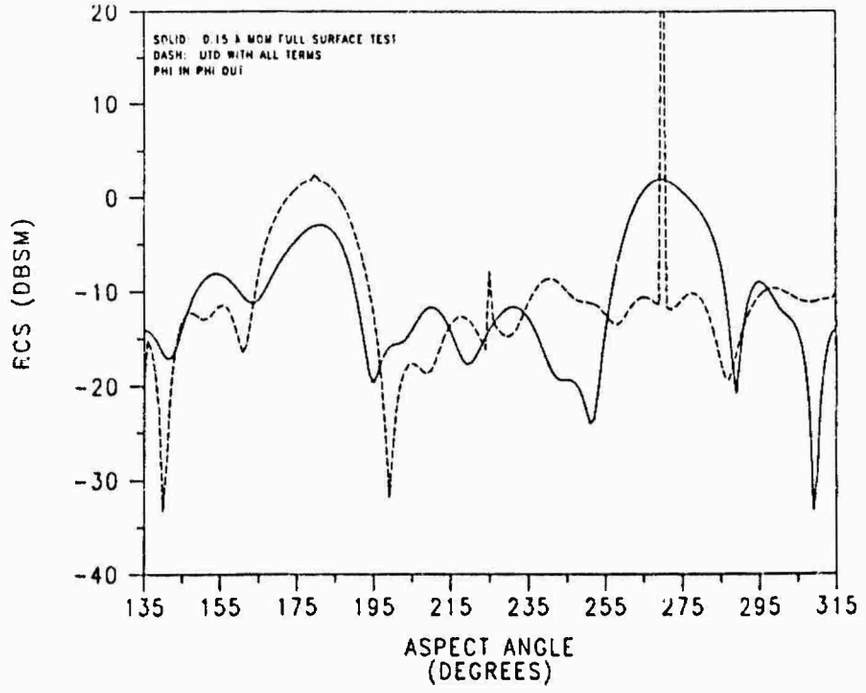

FIGURE 4-24. 90 DEGREE BISTATIC RCS OF 9" DIHEDRAL AT 3 GHZ MOM VERSUS UTD COMPARISON

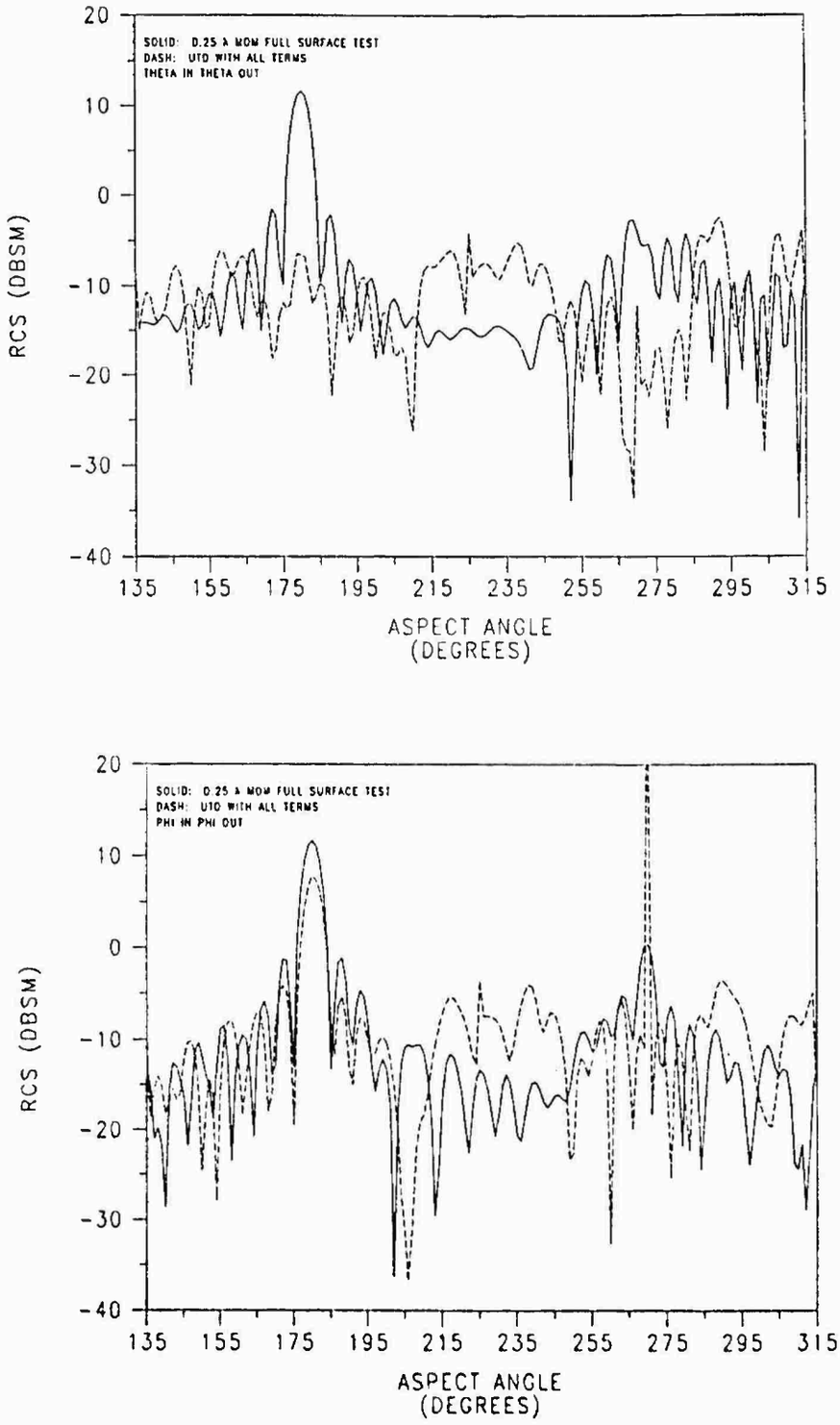

FIGURE 4-25. 90 DEGREE BISTATIC RCS OF 9" DIHEDRAL AT 10 GHZ MOM VERSUS UTD COMPARISON

Model - Measurement Comparison

Figure 4-26 shows the comparison between the MOM with 0.10 wavelength full surface test patch and measurement for the monostatic RCS at 2 GHz for theta and phi polarization. For theta polarization, the agreement was excellent except for the depth of the null at 110°, which was off by only 5 dBsm. For phi polarization, the agreement was good, but not as good as the theta polarization. There were problems with the null depths at 22°, 67°, and 82°, but the difference was at most 5 dBsm. There were other areas of slight discrepancy, but overall the pattern compared well for phi polarization. Figure 4-27 shows the MOM measurement comparison for the theta in phi out cross polarization component. The comparison was very poor between measurement and the MOM for the cross polarization component, especially when compared to the the copolarization comparison. One explanation for the poor comparison is the measurement system was approaching the limit of the noise floor of the receiver. This noise is shown by the jaggedness or roughness of the measured pattern. Error can be introduced into the measurements by the cross polarization characteristics of the transmitting and receiving antennas. Coupling between the transmitting and receiving antennas is also a problem when taking monostatic measurements. Another possible trouble area was that the MOM code had to be run with theta equal to 89° to obtain any cross polarization information. This put the source-receiver 1° (smallest angular increment allowed by the ESP code) off the principal plane. When the code was run at theta equal 90°, the cross polarization component was absent, so the code was rerun with the small change in theta and then the cross polarization appeared. Assuming that the

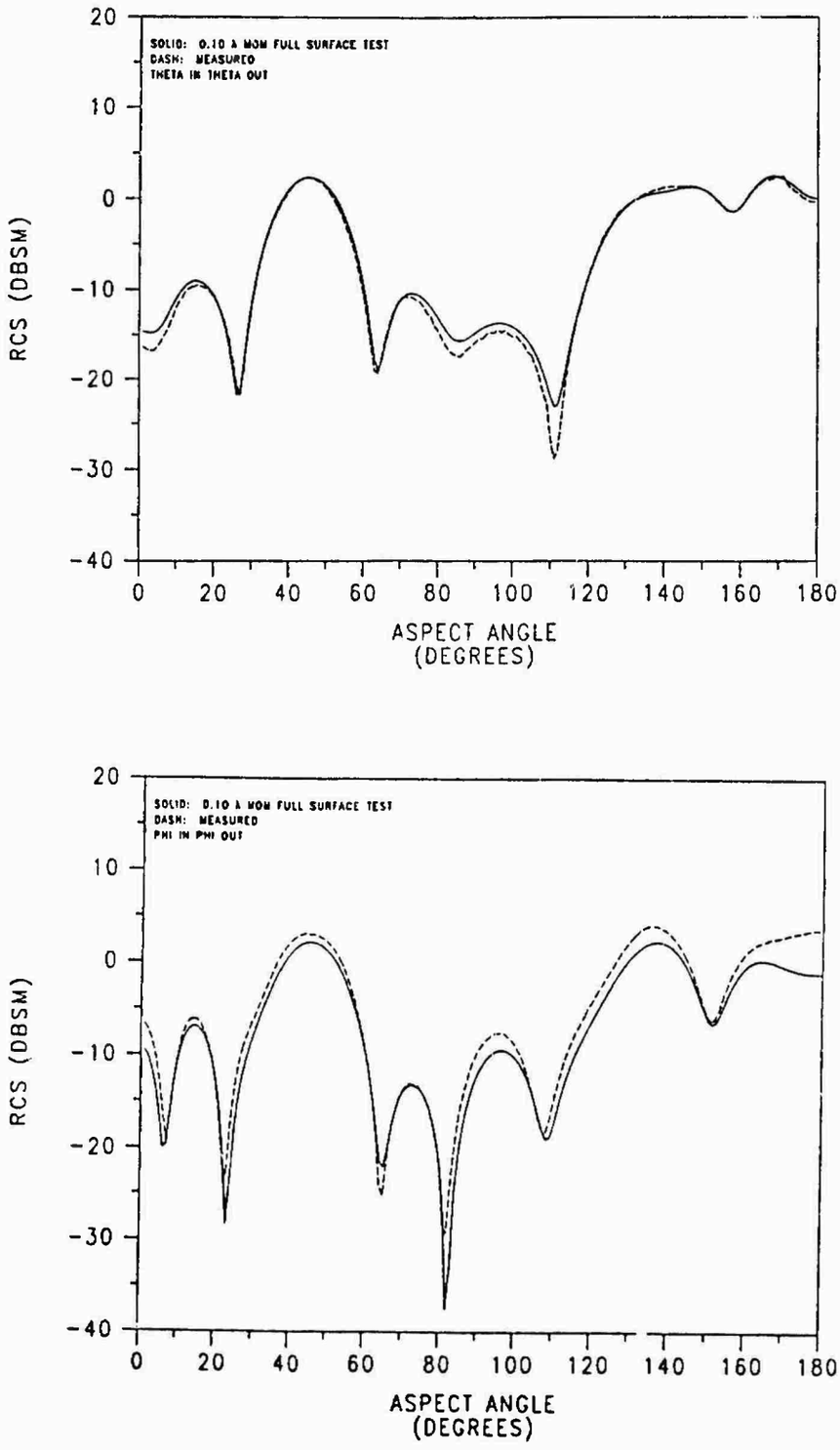

FIGURE 4-26. MONOSTATIC RCS OF 9" DIHEDRAL AT 2 GHZ MOM VERSUS MEASURED COMPARISON

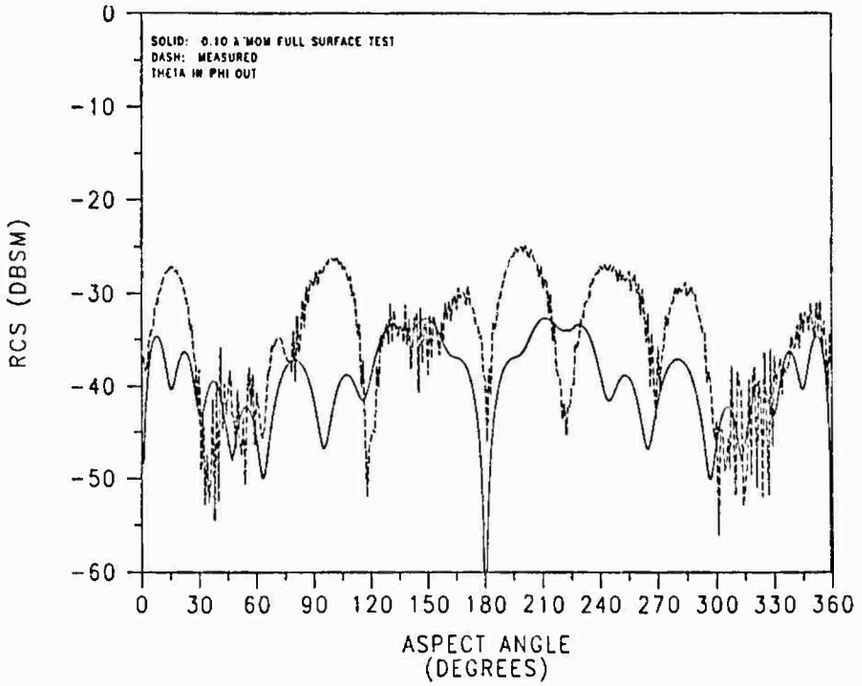

FIGURE 27. MONOSTATIC RCS OF 9" DIHEDRAL AT 2 GHZ
MOM VERSUS MEASURED COMPARISON

measurement system's target mount had a small error in the position of the dihedral, running the code with the 89° angle was not a bad approximation. The relative level of the MOM and measured was not bad, just the actual pattern oscillations.

Figure 4-28 shows the MOM, with 0.25 wavelength full surface test patch, measurement comparison for the monostatic RCS at 10 GHz for theta polarization. The comparison is excellent! The phi polarization pattern was not measured by OSU-ESL, but the MOM solution is shown for completeness. Figure 4-29 shows the cross polarization comparison for theta in phi out polarization. Both measurements were for theta in phi out polarization, and the fact that the patterns were not identical points to problems with the measurement process. The MOM code was run again with theta equal to 89° to obtain cross polarization information. Figure 4-30 shows the phi in theta out polarization MOM solution, for which there was no measurement taken for comparison. For the monostatic case, the theta in phi out polarization pattern is identical to phi in theta out polarization pattern.

Figure 4-31 shows the MOM, with 0.15 wavelength full surface patch test, measurement comparison for the 90° bistatic case at 3 GHz for theta and phi polarization. The comparison for theta polarization is excellent! The phi polarization pattern agreement is good, but not as good as the theta comparison in terms of predicting the depth of the nulls. The phi pattern again has problems in the depth of the nulls at 142°, 162°, 200°, 210°, and 282°. Figure 4-32 shows the cross polarization comparison for theta in phi out and phi in theta out polarization. The comparison is not as good as the copolarization comparisons were. For theta polarization, the patterns

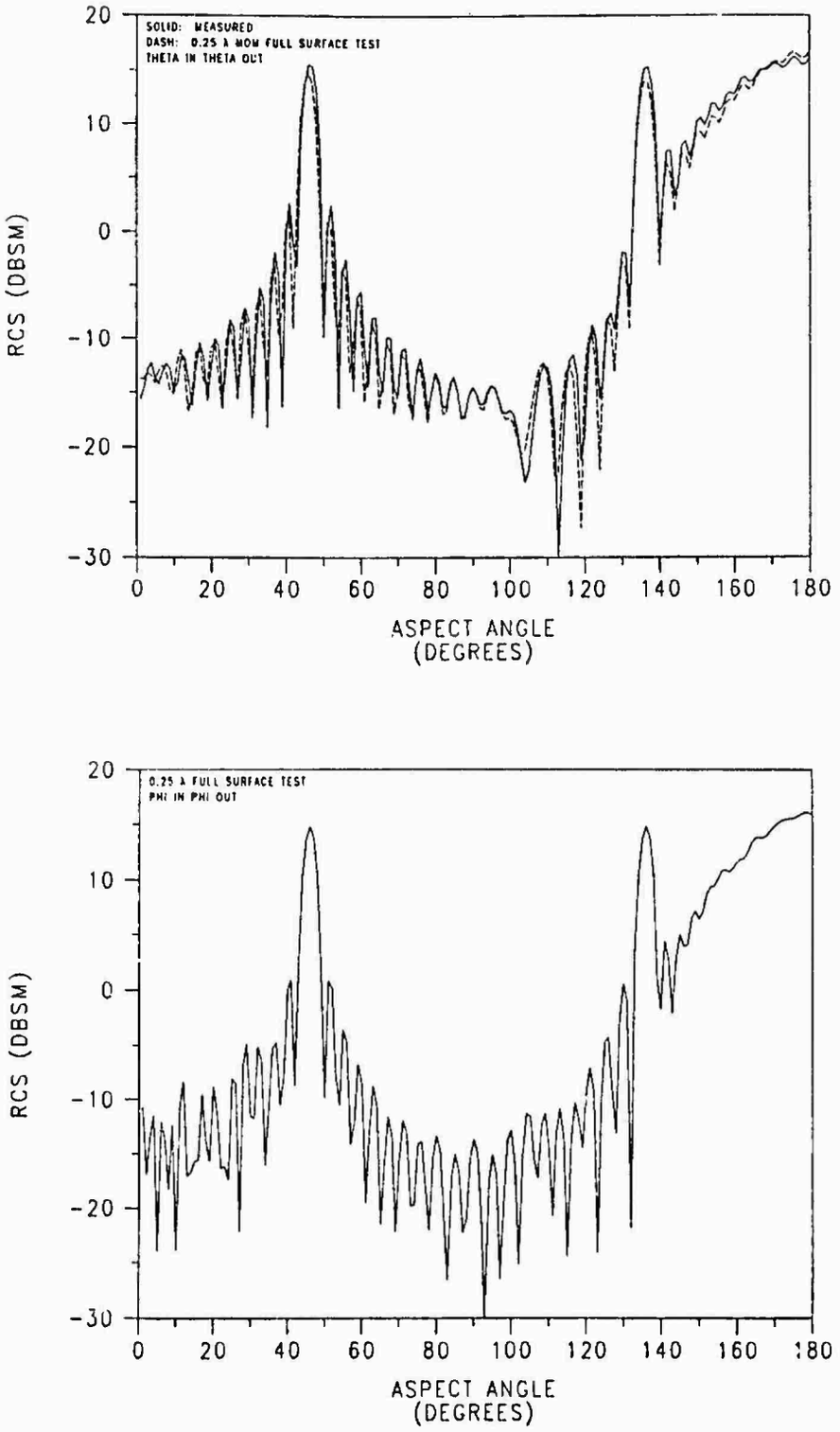

FIGURE 4-28. MONOSTATIC RCS OF 9" DIHEDRAL AT 10 GHZ
MOM VERSUS MEASURED COMPARISON

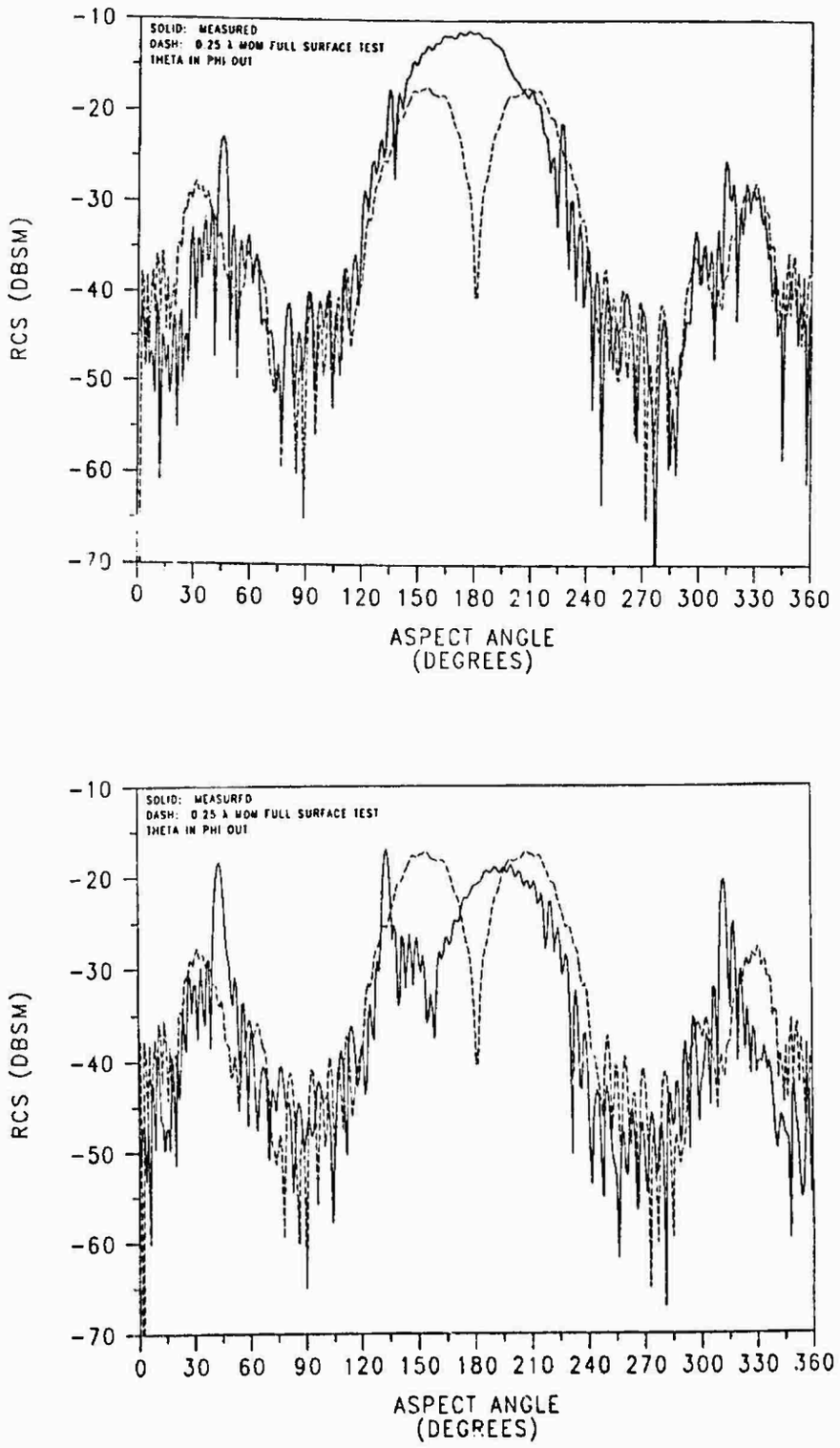

FIGURE 4-29. MONOSTATIC RCS OF 9" DIHEDRAL AT 10 GHZ MOM VERSUS MEASURED COMPARISON

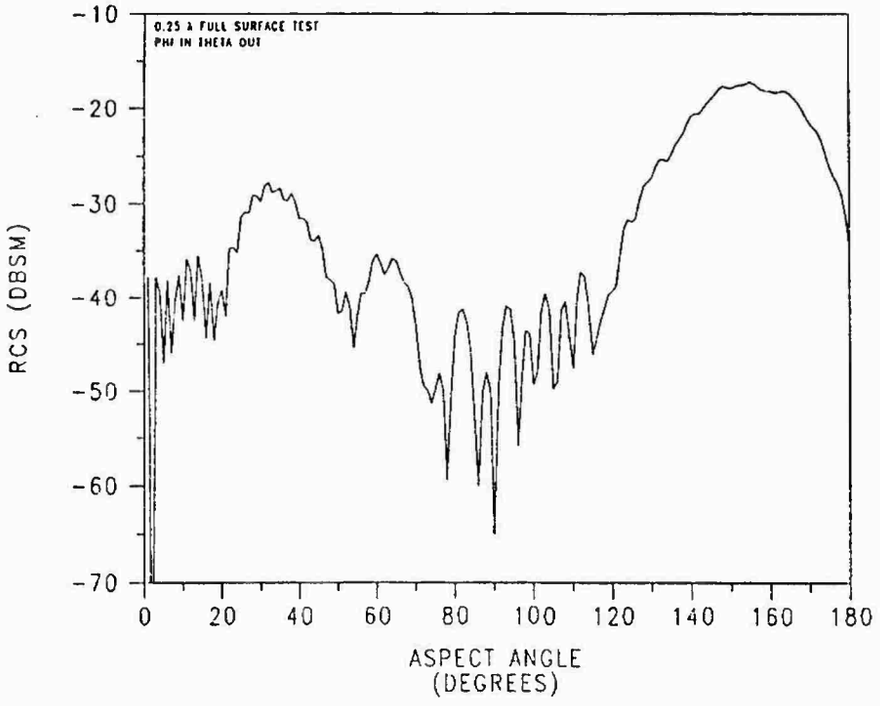

FIGURE 4-30. MONOSTATIC RCS OF 9" DIHEDRAL AT 10 GHZ

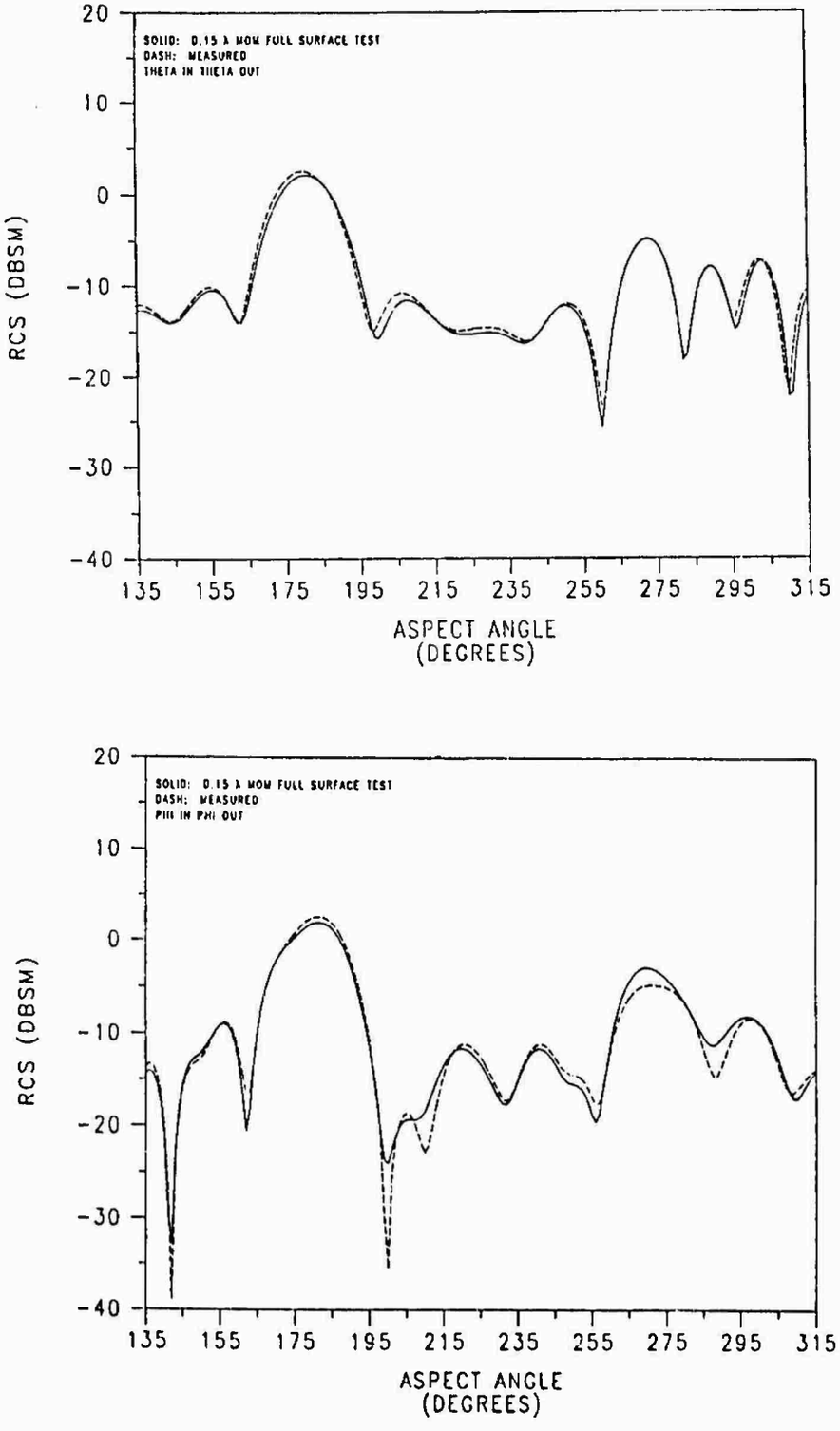

FIGURE 4-31. 90 DEGREE BISTATIC RCS OF 9" DIHEDRAL AT 3 GHZ MOM VERSUS MEASURED COMPARISON

compare well until about 90° where they deviate until 210° when they come together again. For phi polarization, the pattern shapes compare okay, but for some reason the magnitude of the MOM solution is 5 to 15 dBsm higher throughout the pattern. The patterns don't deviate much until the region beyond 330°.

Figure 4-33 shows the MOM measurement comparison for the 90° bistatic case at 10 GHz for theta and phi polarization. The MOM theta polarization pattern compared well with the measured pattern, except for minor differences mostly in the region between 215° and 245°. The MOM and measured patterns for phi polarization also compared well, except for the region near 290° to 295°. Figure 4-34 shows the cross polarization comparison between MOM and measured at 10 GHz. For theta in phi out polarization the peaks were accurately predicted, but the remainder of the pattern didn't compare as well. For phi in theta out polarization the peaks weren't predicted as accurately as for theta in phi out polarization, but the rest of the pattern compared better. The cross polarization comparisons for the bistatic case at 10 GHz were the best out of all of the cross polarization comparisons for MOM versus measured.

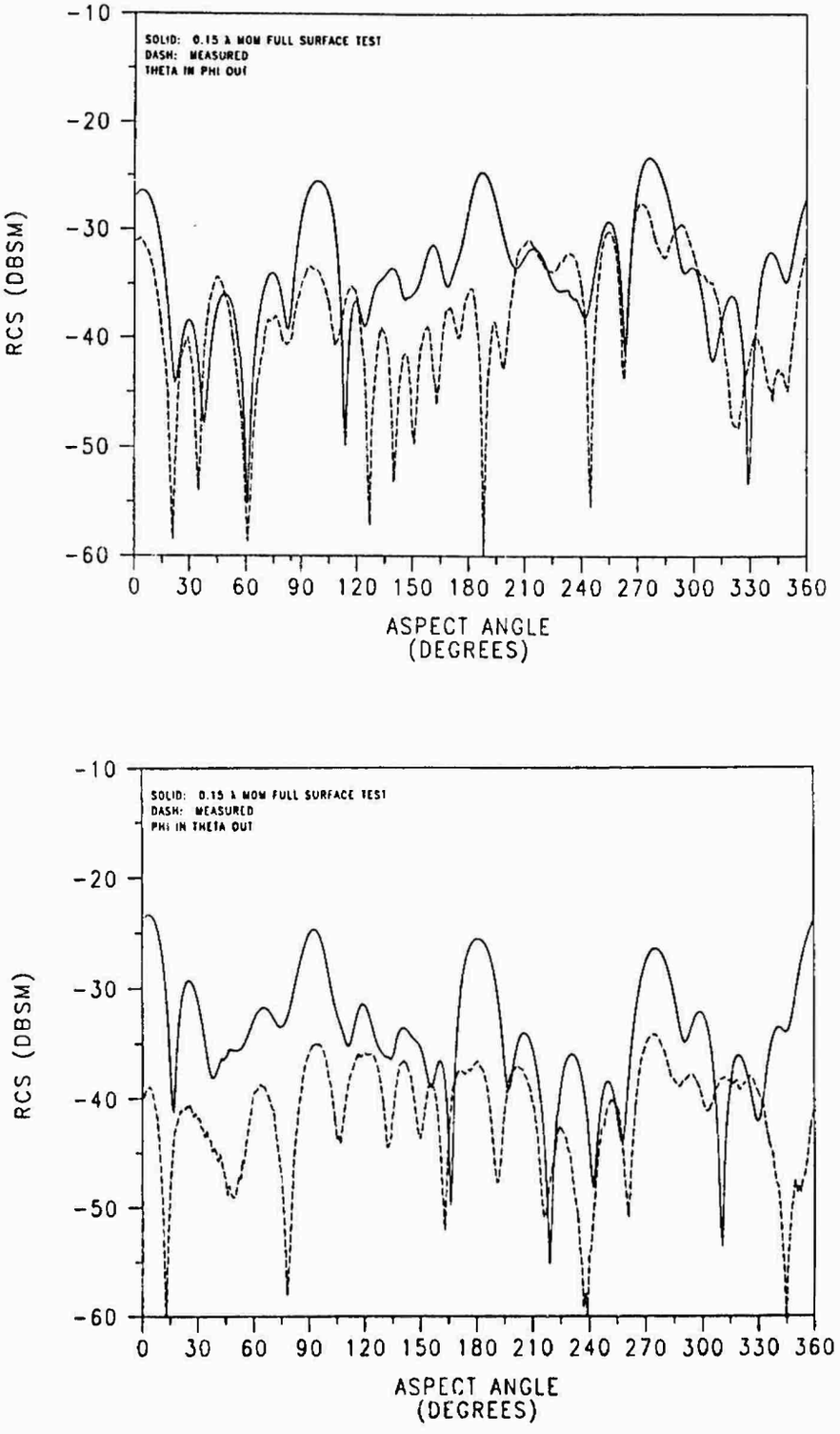

FIGURE 4-32. 90 DEGREE BISTATIC RCS OF 9" DIHEDRAL AT 3 GHZ MOM VERSUS MEASURED COMPARISON

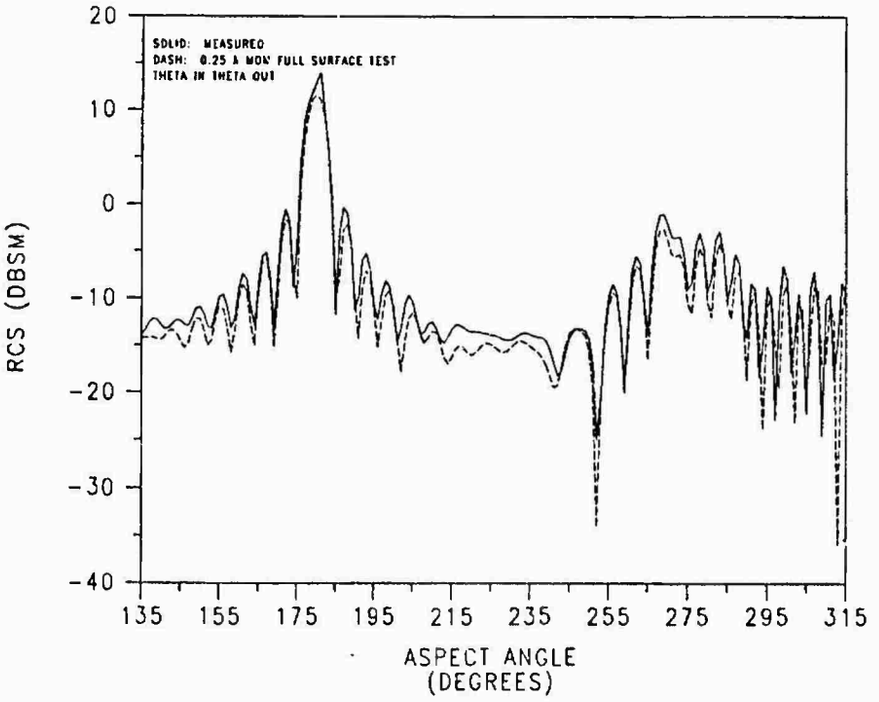

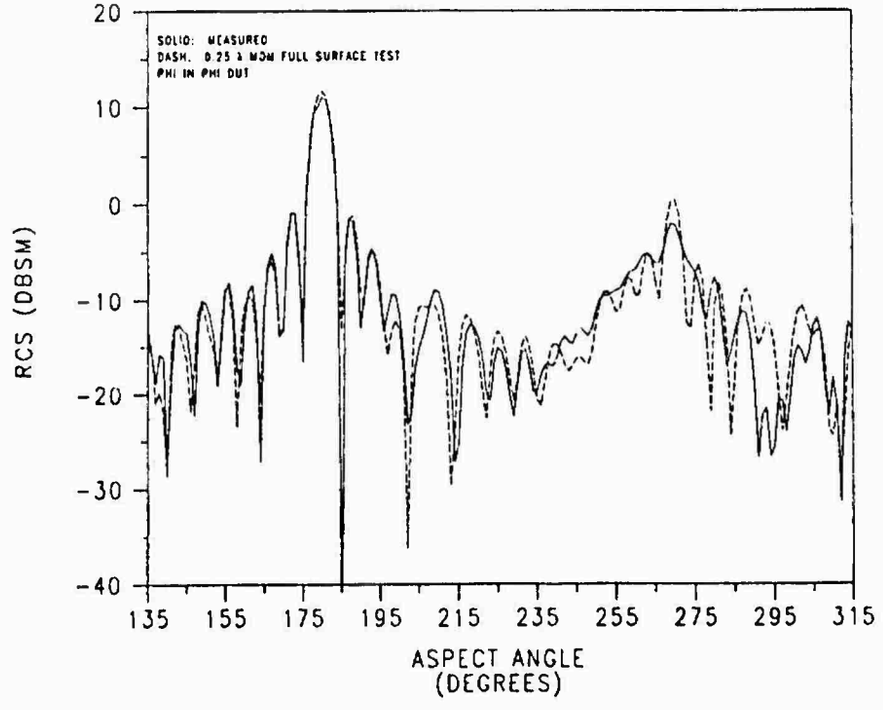

FIGURE 4-33. 90 DEGREE BISTATIC RCS OF 9" DIHEDRAL AT 10 GHZ MOM VERSUS MEASURED COMPARISON

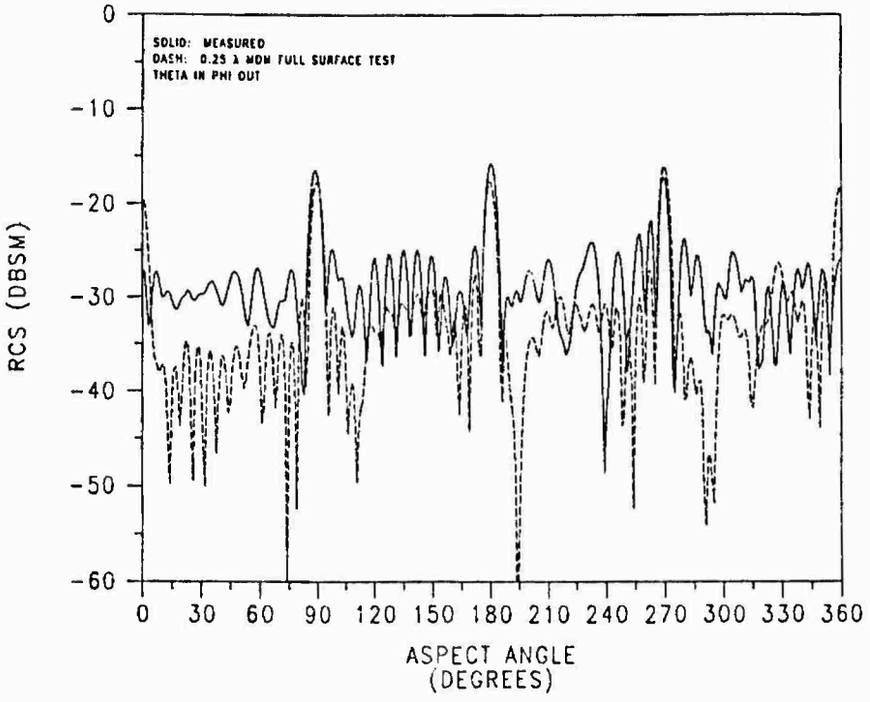

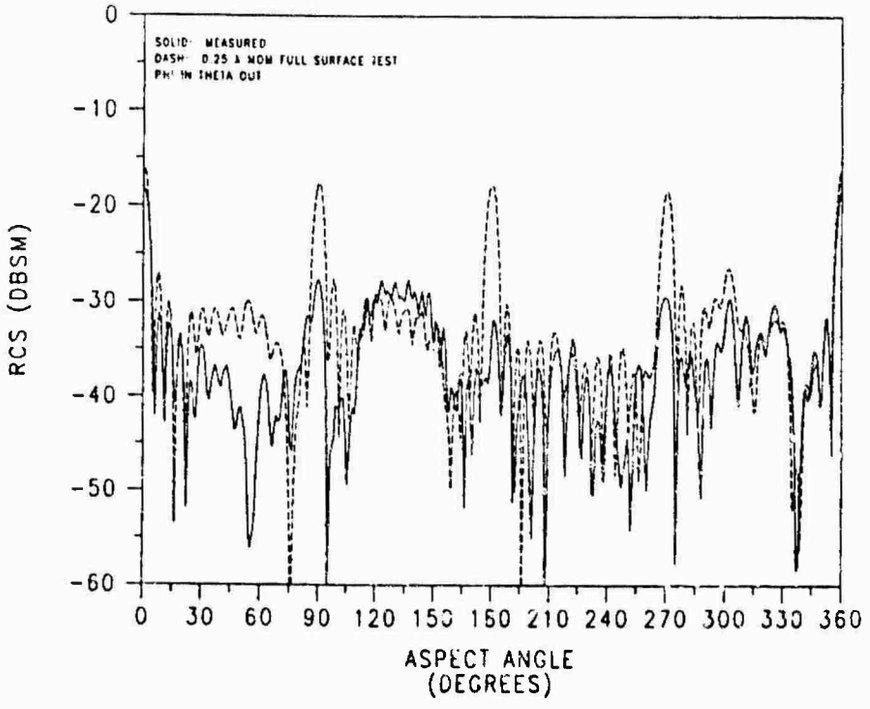

FIGURE 4-34. 90 DEGREE BISTATIC RCS OF 9" DIHEDRAL AT 10 GHZ MOM VERSUS MEASURED COMPARISON

Off Principal Plane Extension

The Electromagnetic Surface Patch code predicted all polarization components accurately for the dihedral corner reflector for the various frequencies and geometries of the measurements. Confidence in the ESP code allows other geometries for the dihedral to be explored. Up to this point all models had been run in the theta equal 89° or 90° elevation plane. What happens to the RCS if the source and receiver is moved off the principal plane? Figure 4-35 shows the RCS for the monostatic case at 3 GHz for theta and phi polarization for various elevation angles. Changing theta from 89° to 75° greatly reduced the backscatter for both theta and phi polarization. However, moving further off the principal plane did not reduce the copolarization backscatter very much. Figure 4-36 shows the cross polarization component of the RCS of the dihedral at 3 GHz for the monostatic geometry. The cross polarization component was lowest for the theta equal 89° pattern. When moving of the principal plane to theta equal 75°, 60°, and 45°, the cross polarization component increased. Also shown in Figure 4-36 is an RCS pattern for the azimuth angle fixed at 145° and the variable angle is elevation (theta). The pattern comparison shows both copolarization and cross polarization for the dihedral at 3 GHz for the monostatic case. For the most part the copolarization components were higher in magnitude than the cross polarization components, but in some regions the cross polarization component was as large and sometimes larger than the copolarization component.

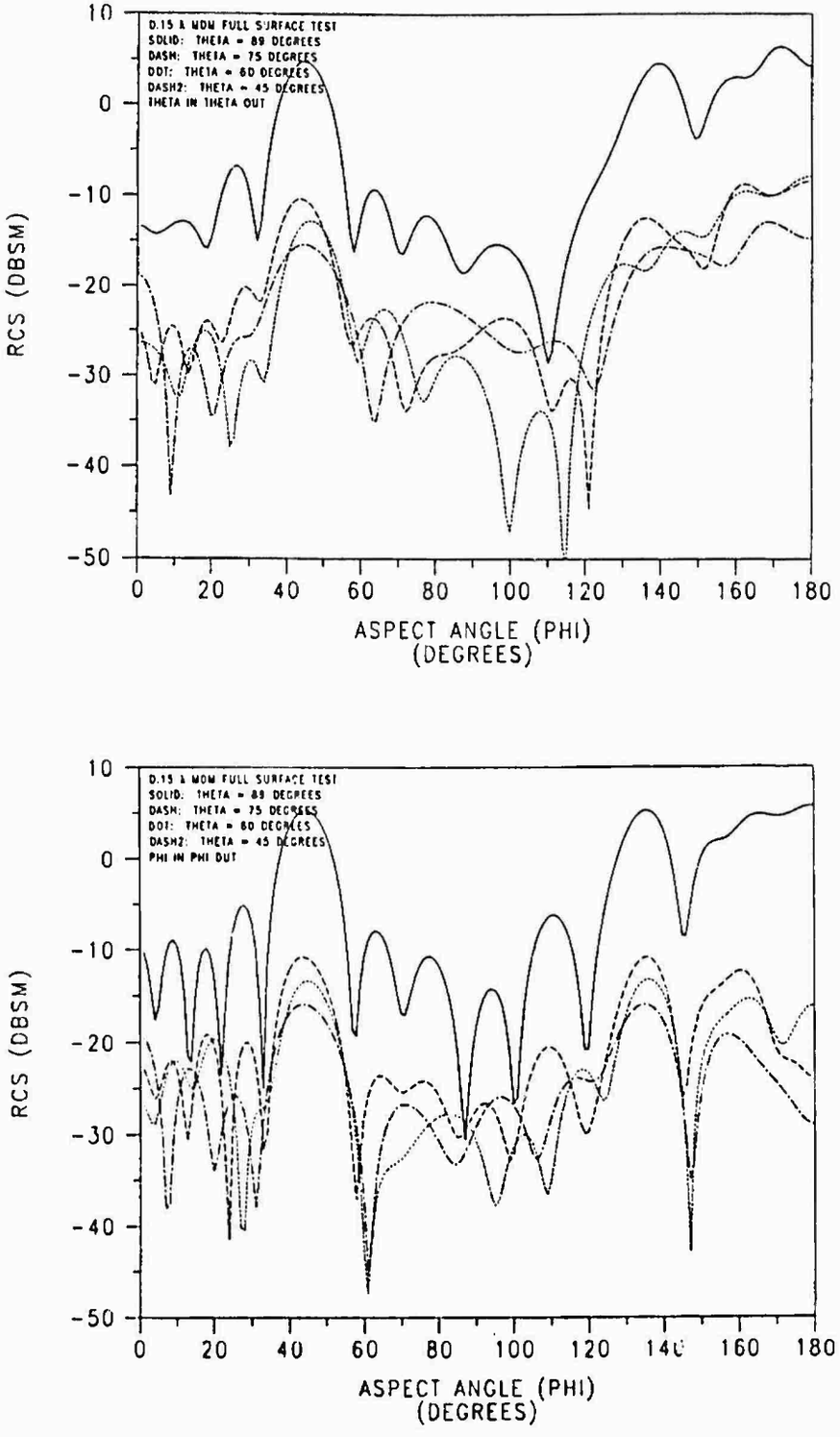

FIGURE 4-35. MONOSTATIC RCS OF 9" DIHEDRAL AT 3 GHZ OFF PRINCIPAL PLANE PATTERN COMPARISON

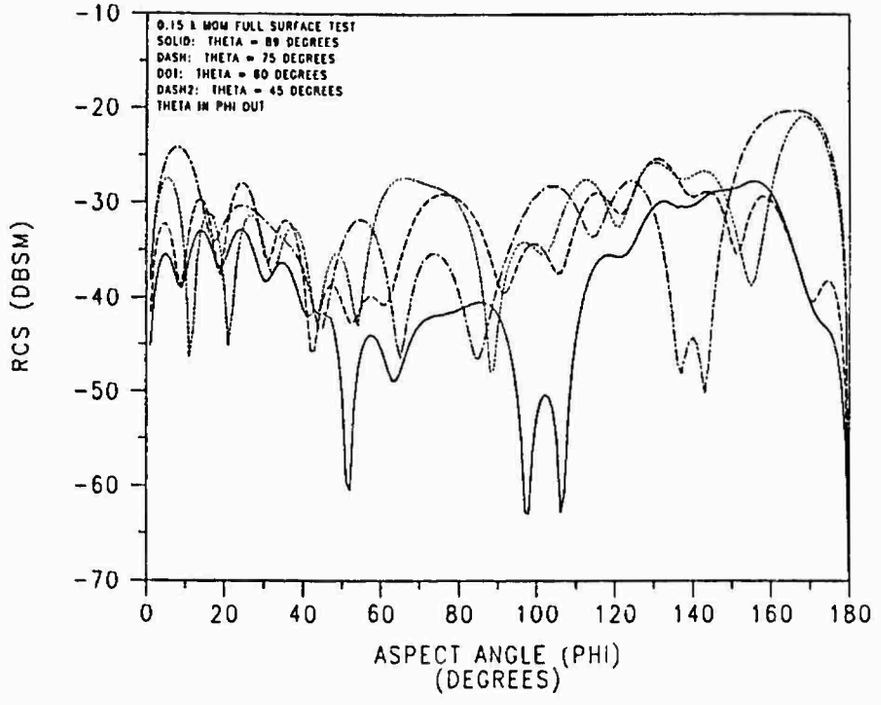

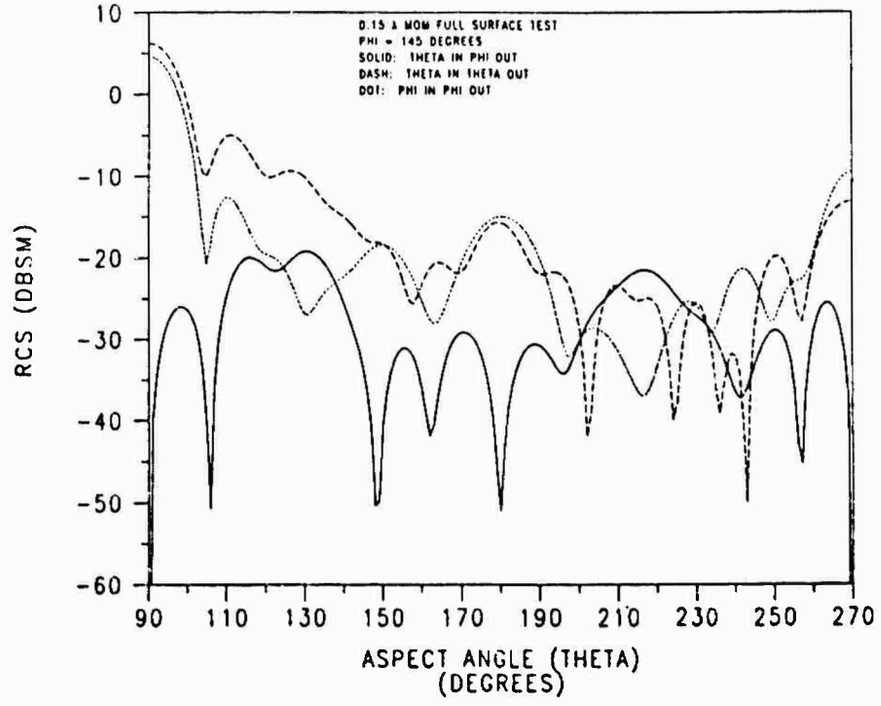

FIGURE 4-36. MONOSTATIC RCS OF 9" DIHEDRAL AT 3 GHZ OFF PRINCIPAL PLANE PATTERN COMPARISON

V. Conclusions and Recommendations

Conclusions

The UTD model employed in this thesis was more efficient in terms of computer time and resource consumption. However, the UTD model was less accurate due to its two dimensional limitation. The two dimensional UTD model didn't accurately predict the RCS of the dihedral corner reflector because the dihedral is a three dimensional object with finite edges and corners. The UTD model ignored some of the diffraction effects which are present in a three dimensional object.

The three dimensional MOM model implemented was more accurate for predicting the RCS of the dihedral corner reflector. But the accuracy of the MOM model was offset by an increased cost of computer time and resource utilization. The MOM provided cross polarization RCS information, whereas the UTD model couldn't predict the cross polarization RCS because of its two dimensional nature. The MOM model had an upper limit in the electrical size of the object it could analyze, translating into a maximum frequency and physical size of the object. Above the maximum frequency and physical size of the object, the MOM model required more resources than the computer had to offer.

The copolarization RCS measurements taken at The Ohio State University ElectroScience Laboratory (OSU-ESL) compared well with the MOM model's results. However, the cross polarization RCS measurements didn't match up with the MOM model as well as the copolarization RCS measurements. The cross polarization RCS

measurements were not as smooth and continuous as expected; instead they exhibited an irregularity which brought doubts as to their accuracy. The magnitudes of the cross polarization RCS measurements weren't too far above the stated noise floor of the OSU-ESL compact range. A problem with cross polarization RCS measurements is the depolarization characteristics of the transmitting and receiving antennas. Coupling is another problem with the antennas when they're in close proximity to each other, as in the monostatic measurements. The target mount which holds the dihedral corner reflector can also introduce error in the measurement due to its depolarization characteristics, especially for bistatic angles.

The MOM model predicted a substantial cross polarization RCS for the dihedral corner reflector when the source and observation point moved away from the principal plane. The dihedral corner reflector would normally be viewed away from the principal plane when used as a component on a complex target model. No off principal plane measurements were taken for comparison, but the accuracy of the MOM model has been verified. A significant cross polarization RCS is desired so that this information can be used as an additional parameter in target identification in future radar systems.

Recommendations

First, the two dimensional UTD model should be extended to the three dimensional problem for the reason that the UTD model is much more efficient in terms of computation time. This extension would be in the area of additional diffraction and reflection mechanisms not incorporated in the two dimensional model. Edge diffraction mechanisms

need to be included for the top and bottom edges of the dihedral corner reflector, whereas the two dimensional model only included diffraction mechanisms for the two outer edges. Corner diffraction mechanisms need to be included if accurate cross polarization information is desired.

Second, the MOM model should be modified to increase the computational efficiency. Different basis (expansion) and testing (weight) functions might reduce the computer time required to compute the impedance and excitation matrices. Entire domain basis functions could possibly reduce the computation time. Symmetry within the impedance matrix might exist, which could be exploited to reduce the number of elements to compute. Another alternative would include the use of a faster computer that has a large core (main) memory. However, modifying the MOM model should be investigated before brute force is implemented.

Third, other computational techniques for electromagnetic scattering should be explored. The Spectral Domain and Conjugate Gradient techniques have been identified as possible alternatives to the UTD and MOM techniques. The first area to examine is the application of the technique to open body surfaces like the dihedral corner reflector. Many techniques are limited to closed body surfaces, such as cylinders and cones.

Finally, other structures should be modeled for cross polarization RCS for both monostatic and bistatic geometries off the principal plane. A flat plate, trihedral corner reflector, cone, cylinder, and ogive are examples of other structures to model. If the object is a closed body surface then other computational techniques become available to the researcher, such as the MOM solution of the Magnetic Field Integral Equation (MFIE).

Summary

This thesis examined the Radar Cross Section (RCS) of the dihedral corner reflector for both monostatic and bistatic geometries. The full polarization of the RCS was maintained while the dihedral corner reflector was modeled on and off the principal (horizontal reference) plane. The dihedral corner reflector was composed of two perfectly conducting 9 inch square flat plates joined along a common edge so that they formed an interior angle of 90 degrees. The frequencies of interest included 2, 3, and 10 GHz. The Uniform Theory of Diffraction and the Method of Moments were utilized in the modeling. The results from the models were compared with measurements for the principal plane RCS. The MOM model was then extended to off principal plane RCS, which was not measured.

Appendix A: Definition of Line Types and Terms

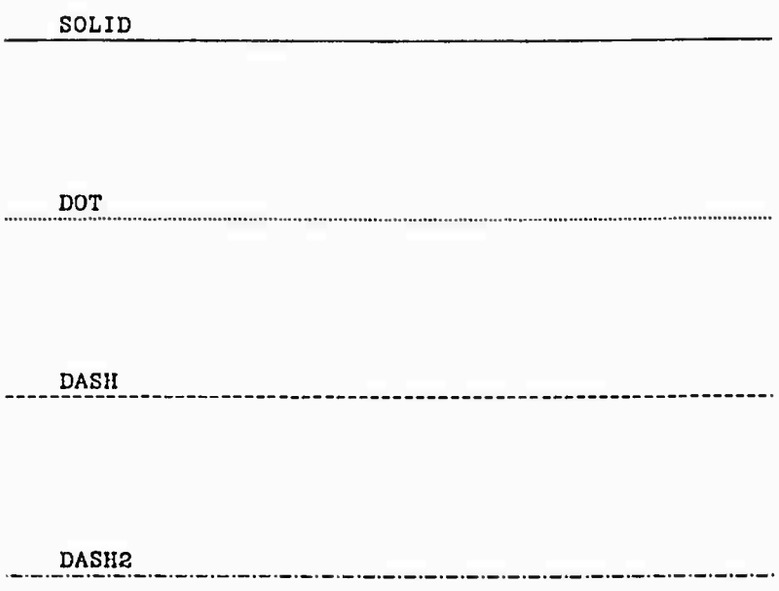

Figure A-1. Definition of Line Types

Definition of Terms

$\underline{\mathbf{E}}$	Complex Electric Field Intensity Vector
$\underline{\mathbf{H}}$	Complex Magnetic Field Intensity Vector
$\underline{\mathbf{J}}$	Complex Electric Current Density Vector
$\underline{\underline{s}}$	Complex Scattering Coefficient
σ	Radar Cross Section
$\hat{h}$	Horizontal Unit Vector
$\hat{v}$	Vertical Unit Vector
$\hat{i}$	Incident Propagation Direction Unit Vector
$\hat{D}$	Diffraction Propagation Direction Unit Vector
$<\underline{\underline{D}}_E(\hat{D},\hat{i})>$	Diffraction Dyadic
D_E	Diffraction Coefficient
$\langle x,y \rangle$	Inner Product
w_m	Weight or Test Function
f_n	Expansion or Basis Function

Appendix B: Measurement Facility

The measurements were performed at the The Ohio State University ElectroScience Laboratory (OSU-ESL) compact scattering range. The compact range is a broadband, coherent, stepped-CW radar measurement facility which has the capability of measuring either the complex scattering spectrum of a target over a broad range of frequencies at a fixed look angle, or of measuring the angular RCS pattern at the fixed frequency. The compact range has the ability to measure both amplitude and absolute phase over an extremely broad band of 1 to 18 GHz.

In either the frequency scan or angular scan mode, each data sample is distilled from a set of four separate measurements:

1) target
2) target background
3) calibration target
4) chamber background

For a target in free space, 2 and 4 are the same; for a target mounted on a ground plane, 2 is a measurement of the scattering of the ground plane alone. An array of these four measurements is stored in the computer and a post facto vector subtraction is used to remove undesired deterministic signals due to the chamber, ground plane, horn coupling, pedestal, etc., from the desired target signal. At each sample, the result is calibrated against the known RCS of the calibration object, usually a sphere. The procedure has been shown to produce excellent results for free space

measurements of a variety of canonical objects. When the measured results are compared to the exact solutions for these objects, the error component is some 30 dB below the target response.

The measurement system is shown in block form in Figure B-1. Data acquisition is controlled by a VAX 11/750 minicomputer. The system presently is able to acquire approximately 4 samples per second in the frequency scan mode and 8 samples per second in the angular scan mode.

The source is a Watkins-Johnson crystal stabilized frequency synthesizer with a transmit power capability of approximately 100 milliwatts (mW). A second Watkins-Johnson is used to downconvert the received signal to 1 GHz, bypassing the down-conversion loop in the Scientific Atlanta receiver and stabilizing the IF noise level. The resulting receiver sensitivity is approximately -100 dBm over the entire band from 2 to 18 GHz.

The antenna feed system uses a pair of broadband, coaxial, TEM horns in a side-by-side configuration at the focal point of a 12' diameter Scientific Atlanta offset reflector to which 4' flared edges designed at OSU-ESL have been attached in order to eliminate the interference of edge effects with the plane wave field. The plane wave illuminated sweet spot is 8' wide by 4' high.

The target is supported on a low cross section metallic pedestal designed at OSU-ESL with a 500 pound capacity and computer controlled rotation capability accurate to within 0.01 degrees. The anechoic chamber is 40 by 20 by 60 feet with ridged absorber on the floor and ceiling, and pyramidal cone panels on the walls.

In a typical frequency scan, the sampling rate is every 10 MHz so that the total open time window is 100 nanoseconds. With the target located some 30' from the back wall and 24' from the main dish, this sampling rate avoids aliasing of the chamber return into the target area. In the most recent version of the radar system, the stepped-CW mode has been replaced by a pulsed stepped-CW mode of OSU-ESL design which uses a set of switches to open and close the transmitter and receiver with a 40 nanosecond wide pulse. With this system, the return from the back wall, main reflector, and direct horn-to-horn coupling is eliminated entirely so that the system can devote nearly all of the -80 dB dynamic range available in the receiver to the target response. In addition, the pulsed system allows one rather than two antennas to be used at the feed, thus improving the focus of the offset fed reflector configuration.

The AEL feed antennas operate from 1 to 12 GHz or 2 to 18 GHz in a single frequency scan. A typical spectral bandwidth of 2 to 18 GHz gives a time resolution of 0.0625 nanoseconds on a spatial resolution of 0.375 inches downrange. A resolution of this magnitude allows the finer details of the target's structural scattering characteristics to be isolated into distinct local scattering centers and diagnosed separately.

The sensitivity of the measurements is ultimately limited not by the noise floor of the receiver but by the clutter floor, which is determined by the ability to achieve the vector subtraction. Since the chamber clutter from points at large distances from the target region may be removed either numerically or electronically with the pulsed system, it is the clutter which returns in or near the target time frame which sets the clutter floor. As stated above, for free space measurements this error has been found to

be approximately 30 dB below the target response. When the target is mounted on a ground plane, it is the ground plane scatter which primarily determines the clutter floor. The subtractability, not just the absolute level, of the ground plane return is the key. Therefore, the stability and positional repeatability of the ground plane are the limiting factors. In the past year, ground plane clutter levels of -55 dBsm absolute have been achieved routinely.

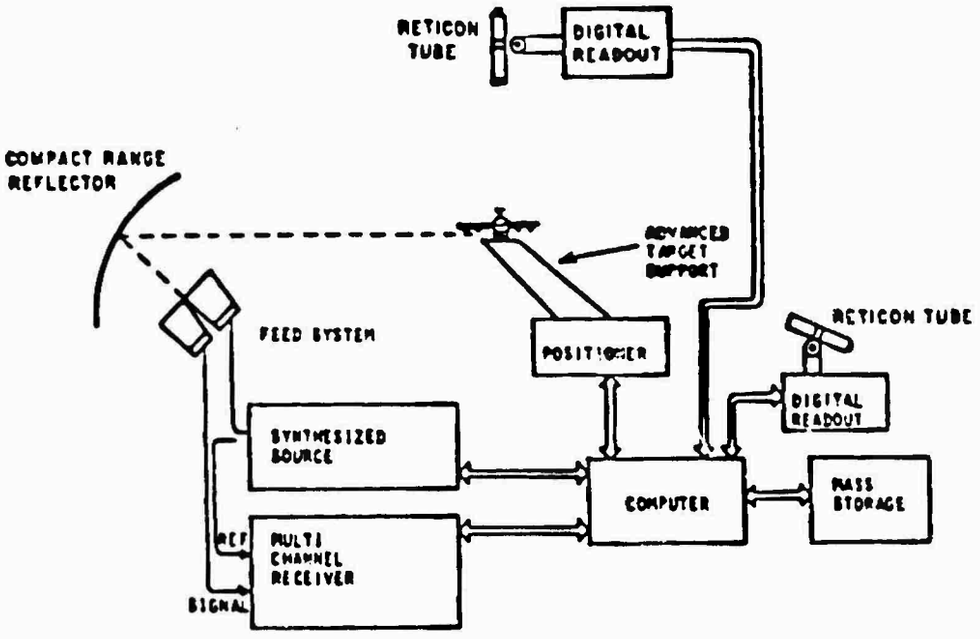

FIGURE B-1. COMPACT RANGE BLOCK DIAGRAM

Bibliography

Aberegg, K.R. UTD Interaction between Plates for Backscatter. MS Thesis, Department of Electrical Engineering, The Ohio State University, Fall 1985.

Baeumler, H.W. and E.M. Kennaugh. "Polarization Properties of Reactive Wall Corner Reflectors." Report 768-3, The Ohio State University Antenna Laboratory, June 1958.

Harrington, R.F. Field Computation by Moment Methods. Malabar: Krieger, 1968.

Hines, J.N. and J.A. McEntee. "Echo Area of Acute Angle Dihedral Corner Reflectors." Report 612-13, The Ohio State University Antenna Laboratory, October 1956a.

-----. "Test of a New Type of Circularly Polarized Corner Reflector with Broad Coverage." Report 612-8, The Ohio State University Antenna Laboratory, July 1956b.

Keller, J.B. "The Geometrical Theory of Diffraction," J. Opt. Soc. Amer., Vol. 52, pp. 116-130, 1962.

Kennaugh, E.M. "Design and Test of a Reflector for the GAR-1 Target." Report 601-13, The Ohio State University Antenna Laboratory, October 1956a.

-----. "A corner Reflector for use with Circularly Polarized Radars." Report 601-8, The Ohio State University Antenna Laboratory, January 1956b.

Knott, E.F. and others. Radar Cross Section. Dedham: Artech House, 1985.

Kouyoumjian, R.G. and others. "A Short Course on The Modern Geometrical Theory of DIffraction." Lecture material and notes. The Ohio State University, Department of Electrical Engineering, September 1985.

-----. "A Uniform GTD for the Diffraction by Edges, Vertices, and Convex Surfaces." The Ohio State University ElectroScience Laboratory, Department of Electrical Engineering, July 1979.

-----. "A Uniform Geometrical Theory of Diffraction for an Edge of a Perfectly Conducting Surface," Proc. of the IEEE, Vol. 62, No. 11, pp. 1448-1461, November 1974.

Marhefka, R.J. "Radar Cross Section Basic Scattering Code, Part I: User's Manual." The Ohio State University ElectroScience Laboratory, Department of Electrical Engineering, September 1984.

Mittra, R. and T.S. Li. "A Spectral Domain Approach to the Numerical Solution of Electromagnetic Scattering Problems." Antenna Laboratory Report No. 72-1, University of Illinois, March 1972.

Newman, E.H. "A User's Manual for Electromagnetic Surface Patch (ESP) Code: Version II - Polygonal Plates and Wires." Technical Report 717067-4, The Ohio State University ElectroScience Laboratory, May 1985.

Sikta, F.A. UTD Analysis of Electromagnetic Scattering by Flat Plate Structures. PhD dissertation, Department of Electrical Engineering, The Ohio State University , December 1981.

Zelnio, E.G. Personal interviews. AFWAL/AARM-3, Wright-Patterson AFB OH, November 1985 through October 1986.

VITA

Second Lieutenant Jeffrey L. Fath was born [redacted] He graduated valedictorian from [redacted] in 1981 and attended [redacted] where he graduated Summa Cum Laude with a Bachelor of Science in Electrical Engineering in June 1985. Upon graduation, he received a commission in the USAF through the ROTC program. He then entered the School of Engineering, Air Force Institute of Technology, Wright-Patterson Air Force Base, Ohio in June 1985.

Current address: [redacted]

Permanent address: [redacted]

UNCLASSIFIED
SECURITY CLASSIFICATION OF THIS PAGE

REPORT DOCUMENTATION PAGE

Form Approved
OMB No. 0704-0188

1a. REPORT SECURITY CLASSIFICATION: UNCLASSIFIED	1b. RESTRICTIVE MARKINGS
2a. SECURITY CLASSIFICATION AUTHORITY	3. DISTRIBUTION/AVAILABILITY OF REPORT: Approved for public release; Distribution unlimited.
2b. DECLASSIFICATION/DOWNGRADING SCHEDULE	
4. PERFORMING ORGANIZATION REPORT NUMBER(S): AFIT/GE/ENG/86D-26	5. MONITORING ORGANIZATION REPORT NUMBER(S)
6a. NAME OF PERFORMING ORGANIZATION: School of Engineering; 6b. OFFICE SYMBOL (If applicable): AFIT/ENG	7a. NAME OF MONITORING ORGANIZATION
6c. ADDRESS (City, State, and ZIP Code): Air Force Institute of Technology, Wright-Patterson AFB, Ohio 45433-6583	7b. ADDRESS (City, State, and ZIP Code)
8a. NAME OF FUNDING/SPONSORING ORGANIZATION: Avionics Laboratory; 8b. OFFICE SYMBOL (If applicable): AFWAL/AARM	9. PROCUREMENT INSTRUMENT IDENTIFICATION NUMBER
8c. ADDRESS (City, State, and ZIP Code): Wright-Patterson AFB OH 45433-6543	10. SOURCE OF FUNDING NUMBERS: PROGRAM ELEMENT NO. 62204F; PROJECT NO. 7622; TASK NO. 08; WORK UNIT ACCESSION NO. 51

11. TITLE (Include Security Classification): See Box 19

12. PERSONAL AUTHOR(S): Jeffrey L. Fath, B.S.E.E., 2d Lt, USAF

13a. TYPE OF REPORT	13b. TIME COVERED	14. DATE OF REPORT (Year, Month, Day)	15. PAGE COUNT
MS Thesis	FROM _____ TO _____	1986 December	108

16. SUPPLEMENTARY NOTATION

17. COSATI CODES			18. SUBJECT TERMS (Continue on reverse if necessary and identify by block number)
FIELD	GROUP	SUB-GROUP	Electromagnetic Scattering, Method of Moments, Polarization Diversity, Uniform Theory of Diffraction
20	03		

19. ABSTRACT (Continue on reverse if necessary and identify by block number)

Title: FULL POLARIMETRIC NON-SPECULAR SCATTERING OF FLAT PLATE STRUCTURES

Thesis Chairman: Andrew J. Terzuoli
Assistant Professor of Electrical Engineering

Approved for public release IAW AFR 190-1.
LYNN E. WOLAVER 5 Mar 87
Dean for Research and Professional Development
Air Force Institute of Technology (AFIT)
Wright-Patterson AFB OH 45433

20. DISTRIBUTION/AVAILABILITY OF ABSTRACT	21. ABSTRACT SECURITY CLASSIFICATION
☒ UNCLASSIFIED/UNLIMITED ☐ SAME AS RPT. ☐ DTIC USERS	UNCLASSIFIED

22a. NAME OF RESPONSIBLE INDIVIDUAL	22b. TELEPHONE (Include Area Code)	22c. OFFICE SYMBOL
Andrew J. Terzouli	(513) 255-3576	AFIT/ENG

DD Form 1473, JUN 86 — Previous editions are obsolete. — SECURITY CLASSIFICATION OF THIS PAGE

UNCLASSIFIED

This thesis examined the electromagnetic scattering of a dihedral corner reflector for both monostatic and bistatic source-receiver geometries. The full polarization characteristics of the electromagnetic scattering was maintained while the dihedral corner reflector was modeled on and off the principal (horizontal reference) plane. The dihedral corner reflector was composed of two perfectly conducting 9 inch square flat plates joined along a common edge so that they formed an interior angle of 90 degrees. The frequencies of interest included 2, 3, and 10 GHz. The theoretical modeling utilized the Uniform Theory of Diffraction (UTD) and the Method of Moments (MOM). The analysis was performed on a Cray X-MP supercomputer and a VAX 11/785 minicomputer. The results from the models were compared with each other, and with measurements for validation. The measurements were taken on the principal plane for same sense and cross polarization components. The MOM model compared well with measurement for the monostatic and bistatic same sense polarization components. However, differences were noted for the cross polarization component comparison. The MOM model was then extended to off principal plane geometries, which were not measured. A substantial amount of cross polarization scattering was predicted for off principal plane geometries.